THE DESIGN OF GAS CHROMATOGRAPHY IONIZATION DETECTORS

A STUDY OF THE ELECTRON CAPTURE DETECTOR AND THE FLAME IONIZATION DETECTOR

By

Martin E. Scolnick

A dissertation submitted in partial fulfillment of the requirements for the Degree of Master of Science in the University of Aston, Birmingham, England

1969

Research Advisor:
Professor F. M. Page

TO MY WIFE, SHARON

For her love and companionship and for the memories we share of a wonderful year in England

ACKNOWLEDGEMENTS

The author would like to express his appreciation to the management of Varian Aerograph and to Mr. C. H. Hartmann in particular, for the opportunity to study at the University of Aston.

Thanks are also due to Dr. Raymond Pecsar for his interest and encouragement in the flame ionization detector studies.

Special thanks are due to Professor F. M. Page for many helpful discussions concerning the physics and chemistry of flames and ionized gases.

TABLE OF CONTENTS

ABSTRACT

Two gas ionization detectors were studied from an instrument designer's point of view. Experimental results indicate that the electron capture detector is sensitive to carrier gas density and to atmospheric oxygen. The finite conductivity of electrode insulators was also found to play an important role in the operation of the E.C.D. at high temperatures. The relation between the internal volume of a concentration detector and chromatographic peak resolution was also examined. The problem of flame ionization detector linearity and loss thereof was studied in terms of ion losses by diffusion and recombination and in terms of combustion efficiency.

The effects of bias voltage and electrode spacing on the operating characteristics of the F.I.D. appear to be explainable in terms of an ion recombination hypothesis. The ultimate roll-off of the F.I.D. response curve, however, can be caused by a loss in the flame's ionization efficiency, as demonstrated by the results of a detector calibration experiment. Distortion of chromatograms due to a transfer of heat from the flame to the collector electrode was also demonstrated experimentally.

I. INTRODUCTION

Gas Chromatography detectors must provide at least two kinds of information: the relative times at which the components of an unknown chemical mixture emerge from the separation column and the relative quantities of each component. In order to provide this information a gas ionization detector must be sensitive to some property of the column effluent so that a change in this property causes the detector to "respond". The detector should have the ability to respond as quickly as the sensitizing property can change in the gas stream emerging from the column, if it is to resolve two successive components whose retention times differ by only a small percent.

A desirable detector characteristic is that of response linearity. A perfectly linear detector is one whose response is directly proportional to some quantitative measure of the sensitizing property. In the case of the flame ionization detector the response is proportional to the rate at which hydrocarbon material is carried into the detector flame by the column effluent. In the case of the electron capture detector, however, the response is a non-linear function of the concentration of certain classes of compounds in the column effluent. The flame ionization detector is classified, therefore, as a linear mass rate detector, while the electron capture detector is considered to be a non-linear concentration detector. By measuring a detector's response to known quantities of the sensitizing property, the detector can be calibrated. This thesis is, to a large extent, an investigation into the relationships between the design of a detector and its response characteristics as obtained from calibration data.

II. GAS IONIZATION DETECTORS

The "response" of a gas ionization detector takes the form of an electric current. The detector must include a means of generating ions and/or free electrons and a means of collecting them. The collection of charged particles is accomplished by the use of at least two electrodes whose voltage difference is maintained by a suitable battery, power

supply, or pulsed voltage source. The electric field between the electrodes causes the charged gaseous particles to drift in a direction that is determined by the charge (positive or negative) on the particles and the direction of the field. In general, the current density for charged particles of one sign and one species (i.e., electrons or a particular ion) in the inter-electrode space can be expressed as

$$j = q\,n\,(u\,E + V), \qquad (1)$$

where j is the current density in amp/cm^2, q is the charge in coulombs of the species whose number density is n and whose mobility in $cm^2 sec^{-1}$ volt is u. E is the electric field in volt cm^{-1} and V is the gas velocity in $cm.sec^{-1}$. In general, j is a vector function of the space coordinates x, y and z and of time. The important point here, however, is that equation (1) will enable us to be more specific as to the nature of the sensitizing property.

III. THE ELECTRON CAPTURE DETECTOR

The Electron Capture Detector (E.C.D.) exploits the dependence of n and u in equation (1) on the nature of the carrier of negative charge. Figure 1 shows two basic E.C.D. design geometries. The parallel plate detector, first described by Lovelock and Lipsky (1) in 1961, will serve to illustrate the principle of operation. N_2 carrier gas flows from the column into the volume bounded at the top by a negatively biased radioactive foil electrode and at the bottom by the collector electrode. Both electrodes are in the form of flat disks with holes in them to permit the flow of gas and are separated by an electrical insulator which makes a gas-tight seal with the electrodes. The beta particles emitted from 250 millicuries of tritium in the form of titanium tritide on a stainless steel backing have an energy distribution whose maximum is 18 kev. and which is dissipated by ionizing the N_2. About 175 ion-electron pairs are produced per beta (2). According to Von Engle (3), the ions are of the form N_2^+, N_3^+ and N_4^+. Nitrogen does not form stable negative ions (4), however, so that free electrons in the inter-electrode space are driven against the gas flow to the collector electrode where a current can be monitored. When the column effluent contains mole-

cules with a positive electron affinity, negative ion formation is possible. In this case a fraction of the total number of negatively charged particles in the inter-electrode space are ions and hence have a lower mobility by at least a factor of 10^3. (See, for example, the discussion of the Compton-Langmuire equation in the text by Cobine (5)).

Due to their relatively slow drift speeds negative ions spend more time in the inter-electrode region so that their chances for becoming neutralized by re-combination with the positive nitrogen ions are much greater than those of the free electrons. The net result of introducing electron acceptor molecules into the E.C.D. is, therefore, to reduce the effective values of n and u in equation (1) with a corresponding loss in the current density, j. The sensitizing property, to which the E.C.D. responds is, therefore, the ability of a gas to form negative ions by electron attachment. The detector's response consists of a reduction in the collector current.

Response Characteristics

The earliest attempt to describe the E.C.D.'s response characteristics is the Beer's Law interpretation due to the detector's inventor, J. E. Lovelock (6). This model is based on electron attachment phenomena, as discussed in the text by Healey and Reed (7). Stated briefly, the detector response, S, is related to the concentration of electron capturing species according to the following equation:

$$S/I_o = 1 - \exp(-k \times C) \qquad (2)$$

where I_o is the detector current in the absence of electron acceptors and S is the loss in current due to the presence of the capturing species whose concentration is C. x is a characteristic dimension of the detector. For the parallel plate geometry shown in Figure 1, x is the distance between the electrodes minus some length to account for the fact that most of the free electrons are produced by energetic beta particles some distance away from the radioactive foil. The constant k can be defined by stating that the product k C is the electron attachment coefficient per unit length of drift through a gas that contains a concentration, C, of capturing species. The product k x is often referred to in gas chromatography literature as the "capture coefficient".

In 1962 Wentworth and Becker (8) published a theory of E.C.D. operation that was based on the assumption of an equilibrium between neutral gas molecules, free thermal electrons, and negative ions.

$$A + e \rightleftharpoons A^- \qquad (3)$$

$$K = [A^-] / [A][e] \qquad (4)$$

where A represents the neutral molecule and K is the equilibrium constant for equation (3). If $[e]_o$ is the concentration of thermal electrons inside the detector when the electron capturing species is absent and $[A]_o$ is the concentration of electron acceptors in the gas before it enters the detector, we can write:

$$[A]_o = [A] + [A^-] \qquad (5)$$

$$[e]_o = [e] + [A^-] \qquad (6)$$

Using these expressions in equation (4) and rearranging terms, we get:

$$[A^-] = K\left([A]_o - [A^-]\right)\left([e]_o - [A^-]\right) \qquad (7)$$

Under the assumption that $[A^-] << [A]_o$, equation (7) can be written:

$$[A^-] = K[A]_o\left([e]_o - [A^-]\right) \qquad (8)$$

To relate equation (8) to the E.C.D. response, we first note that the response is a change in the collector current which consists predominantly of free electrons. Equation (1) shows that this current is proportional to the density or concentration of free electrons in the inter-electrode region. We can write, therefore:

$$I_o \backsim [e]_o$$

$$I \backsim [e]$$

$$S = I_o - I$$

where I_o and S have their previous meanings and I is the collector current when electron acceptors are present in the detector. After re-arranging the terms in equation (8) and using equation (6) to eliminate $[A^-]$, we get:

$$K[A]_o = \left([e]_o - [e]\right) \Big/ \left([e]_o + [e] - [e]_o\right)$$

$$K \left[A\right]_o = \frac{S / I_o}{1 - S / I_o} \qquad (9)$$

For comparison the Beer's law in equation (2) can be solved as a function of k x C.

$$k \times C = -\ln (1 - S / I_o) \qquad (10)$$

Design Principles

Both of the above interpretations describe a concentration detector. In both equations, (9) and (10), the independent variable is the ratio S/I_o, or normalized response. It may also be noted that for $S/I_o << 1$ both equations are approximately linear relations between the concentration and the normalized response.

The E.C.D.'s classification as a concentration detector determines how it can be used for quantitative work. In general, the rate at which a gaseous material passes through the detector is given by:

$$\dot{m} = Q C, \qquad (11)$$

where $\dot{m}$ is the flow rate of material in gm/sec, Q is the volume flow rate of the carrier gas in cm^3/sec and C is the concentration of material in gm/cm^3. For column effluent materials C is a function of time. $\dot{m}$ can be expressed as a function of the normalized detector response by using equation (9) or (10) (both equations give essentially the same results for $S/I_o < 0.1$). The integral of $\dot{m}$ over the time interval that it takes for a chromatographic peak to elute is equal to the total weight of the compound that corresponds to the peak. For concentrations that are sufficiently small so that the maximum value of S/I_o is much less than unity, we can use the linear approximation of equation (10) to write:

$$M = \int \dot{m}\, dt = Q \int C\, dt \approx (Q/KI_o) \int S\, dt \qquad (12)$$

where M is the total weight of the sample component whose electron capture coefficient is K. The integrated detector response in equation (12) is equivalent to the area under the chromatogram of the compound in question. Equation (12) implies that for a fixed quantity, M, the chromatographic area is inversely proportional to the carrier gas flow rate, Q. This is a consequence of the fact that the E.C.D. is a concentration detector.

In order for the relation implied by equation (12) to be valid so that chromatograms obtained with different carrier gas flow rates can be compared, for example, it is desirable to minimize the effects of gas flow rate on the standing current, I_o.

Oxygen Back Diffusion

Detection is normally the last step in a chromatographic analysis. Most detectors, therefore, have an exhaust port through which carrier gas and detected samples are vented directly into the atmosphere. Atmospheric O_2, however, is sufficiently electronegative to produce a response in the E. C. D. (30).

It has been shown (9) that when atmospheric O_2 is prevented from back diffusing into the detector through the exhaust port, that the standing current, I_o, is insensitive to changes in the carrier gas flow rate, as long as the detector pressure is held constant.

To prevent O_2 back diffusion from occurring, the detector can be housed in an enclosure which eventually fills up with vented carrier gas. A loose fitting lid on the enclosure provides for access to the detector while permitting the vented gases to finally escape into the atmosphere. To prevent detected samples from back diffusing into the detector, the enclosure can be supplied with an auxilliary flow of inert gas. Another solution is to use a small diameter exhaust port so that the gases are vented with a high linear velocity. In this case, however, an apparent flow sensitivity may occur as a result of the detector's pressure sensitivity.

Experimental Evidence of O_2 Back Diffusion

Figure 2 shows six standing current versus voltage curves for the concentric cylinder E.C.D. shown in Figure 1. In this case the detector was provided with a threaded cap in which a 0.15 inch long, 0.045 inch diameter exhaust port was drilled. The curves were obtained at three different carrier gas (N_2) flow rates. At each flow rate the standing current was measured with and without the detector enclosure lid in place. A 12 millicurie Ni^{63} radioactive foil was used in the detector whose temperature was maintained at $30^{o}C$. The effect of O_2 back diffusion is clearly evidenced by the

fact that at each flow rate the standing current is higher with the lid on. The difference between the curves obtained at different flow rates, however, is due to the combined effects of detector pressure and O_2 back diffusion, as can be seen by a comparison with Figure 3.

The curves in Figure 3 were obtained with a smaller diameter exhaust port (0.01 inches). Here we see that the standing current is completely insensitive to the concentration of O_2 in the detector enclosure, as the presence of the lid has no effect. The increase in current with carrier gas flow rate can be attributed to an increase in detector gas pressure (9).

In the case of the concentric cylinder detector the standing current can be described as a function of voltage (9) by

$$I_o = A\,V / (V + B), \qquad (13)$$

where A is the upper limit for the standing current that is approached as the voltage, V, is made large relative to the parameter B (B is of the order of 1 volt). Measurements at different detector pressures and temperatures show an approximately linear relation between A and the density of carrier gas in the detector. Figure 4 is a plot of the upper limit for the Ni^{63} concentric cylinder detector versus the gas density. The slope of the line in Figure 4 is 1.2×10^{-9} amp per (mm Hg $^{o}K^{-1}$). Therefore, the difference in the two upper curves in Figure 3 can be attributed to a 40 mm Hg change in the detector gas pressure.

Choice of Construction Materials

As noted previously, both the Beer's law of Lovelock's interpretation and the Wentworth-Becker equilibrium theory relate the concentration of detectable substance to the normalized response S/I_o. The choice and condition of the materials used for electrical insulation can play an important role in determining the apparent magnitude of the standing current, I_o.

Electrical Insulation

Figure 5 is a schematic representation of the E.C.D. electric circuit, including the cathode insulation R_1, the resistance of the insulator which separates the cathode from the collector, R_2, and the resistance of the material which insulates the collector from ground, R_3. The voltage source, E, is often a high impedance device so that insufficient insulation at R_1 may cause the cathode potential to drop because of voltage supply overloading. Unless a vacuum tube voltmeter is used, cathode voltage measurements may only be valid when the effective impedance of the voltmeter is present between the cathode and ground. However, leakage currents through R_1 during detector operation present no problem as long as the cathode potential remains constant.

E.C.D. standing currents are typically less than 10^{-7} amp. When a low input impedance device, such as the DC operational amplifiers used by Varian Aerograph, is used for measuring the collector current the difference in potential between collector and ground is often of the order of micro volts or less. In this case the finite conductivity of R_3 presents no problem unless, of course, R_3 is a "dead short".

By far the most serious electrical insulation problem in the design of an E.C.D. is that presented by the inter-electrode insulator. Current that is conducted through this material or across a film of contamination on its surface, such as fingerprints or column bleed condensation, can cause the standing current to appear much larger than its true value. In general, the apparent standing current, I'_o, can be expressed as:

$$I'_o = I_o + V / R_2 \qquad (14)$$

where V is the voltage drop across the inter-electrode insulator and R_2 is the total resistance of the insulator plus contamination (insulator and contamination can be thought of as resistors in parallel). The resistance of clean glass and ceramic insulators decreases exponentially with reciprocal absolute temperature.

$$R \sim \exp (E / R T), \qquad (15)$$

where, according to Jones (10), the activation energy, E, is of the order of 20 k cal/mole. Figure 6 shows the resistance-temperature characteristics of the glass insulator that separated the electrodes of the concentric cylinder E.C.D. that was used in these detector studies. The data were obtained after removing the Ni^{63} radioactive foil. A least squares fit analysis showed that the data are described by:

$$R = 1.59 \exp (121 \times 10^{10}/RT) \text{ Ohms} \qquad (16)$$

with a relative standard deviation of 15%. The activation energy, 121×10^{10} ergs (29.0 k cal) per mole is consistent with the figure quoted by Jones.

The upper curve in Figure 7 is a plot of the apparent (i.e. measured) standing current I_o versus cathode potential for a Ni^{63} concentric cylinder E.C.D. at 342°C. The resistance of the inter-electrode glass insulator at this temperature is 3.35×10^{10} ohms. The conductivity of this insulator is not small in comparison to the conductivity of the ionized gas and is responsible for the linear increase in current that appears in the data for V > 10 volts. The lower curve in Figure 7 is a plot of the true standing current, I_o, that was obtained by subtracting the Ohm's law current from the measurements.

Geometric Considerations

In this section the geometry and internal volume of concentration detectors will be examined in terms of the effects they have on the shape of a chromatogram. A chromatogram that is obtained with the use of a calibrated and well designed detector is a record of the time distribution of detectable substances in the column effluent. On the other hand a detector whose internal volume is too large and whose internal geometry is improperly designed can produce a distorted picture. The following analysis illustrates some of the problems associated with the "mixing chamber effect."

Consider the detector whose internal geometry and gas flow pattern are sketched in Figure 8 and assume that the vortices in the flow pattern provide perfect mixing for gases entering the detector. The rate of change of the total mass of a particular gas in

the detector is equal to the difference between the input and exhaust rates for that gas.

$$d(C\,V)/dt = Q\,C_i - Q\,C \qquad (17)$$

where V is the internal volume of the detector (a constant) and C is the concentration of gas in gms cm^{-3} inside the detector. C_i is the concentration of gas as it enters the detector and Q is the gas flow rate through the detector in cm^{-3} sec^{-1} (we assume that the pressure drop across the detector is negligible). Suppose that C_i is a Gaussian function of time:

$$C_i = C_o \exp\left[-(t-t_o)^2 / 2\sigma^2\right] \qquad (18)$$

where t_o is the retention time and σ is the peak width at 60.6% of its maximum concentration, C_o. Equation (17) can now be written:

$$dC/dt = (C_o/\tau)\exp\left[-(t-t_o)^2/2\sigma^2\right] - C/\tau \qquad (19)$$

where $\tau = V/Q$, is the detector time constant. Equation (19) is linear in C and has the solution

$$C(t) = C_o \sqrt{2\pi}\,(\sigma/\tau)\exp(-2\sigma/\tau)\exp(-\sigma^2/2\tau^2)\int_{-\infty}^{x(t)} \exp(-x^2/2)dx \qquad (20)$$

where $x = (t-t_o)/\sigma - \sigma/\tau$. The integral in equation (20) can be evaluated by the use of error function tables.

The derivation of equation (20) can be found in a paper by James C. Sternberg (11) who also shows the effects of the time constant on the peak height, peak width, and apparent retention time of the concentration distribution as observed from inside the detector. In particular, Sternberg shows that for a ratio, $\tau/\sigma = 1.0381$, the concentration inside the detector maximizes at only 77% of the input maximum, C_o, and lags behind the input distribution by $0.7135\,\sigma$. As τ/σ approaches zero, these figures improve. For example, at $\tau/\sigma = 0.1923$ the concentration inside the detector maximizes at $0.98\,C_o$ and the lag time is down to $0.2\,\sigma$. In practice the width of the concentration distribution eluting from a 5-ft. x 1/8-inch column in a 30 cm^{-3} min^{-1} carrier gas stream is often of the order of 5 seconds (chart recorders are usually limited to a full scale pen deflection in one second, which corresponds to a peak width of approximately two seconds). Therefore, in order to

design an E. C. D. (or any other concentration detector for that matter) so that $\tau/\sigma < 0.2$ we need:

$$\tau = V/Q < 0.2\sigma$$

or $$V < 0.2\sigma \quad Q = 0.5 \text{ cm}^3$$

Equation (20) can be used to plot the concentration inside the detector as a function of time. Sternberg shows curves for the cases $\tau/\sigma = 0,\ 0.2,\ 1.0,\ 5,$ 10 and 20. In general, as τ/σ increases from the ideal optimum value of zero, C (t) becomes broader and non-symmetrical. However, as an approximation for the case of the Gaussian input function, the width of C (t) can be taken as inversely proportional to its height. That is, as C_{max} goes from 0.98 C_o to 0.77 C_o the width of the C vs t curve at 60.6% C_{max} can be expected to increase by a factor of $0.98/0.77 = 1.27$. A broadening of the function C (t), will of course result in broader chromatograms with a consequent loss in peak resolution.

IV. THE FLAME IONIZATION DETECTOR

The Flame Ionization Detector (F.I.D.) makes use of the fact that ions are produced in the process of hydrocarbon combustion. The essential components of this detector are shown in Figure 9. Column effluent gases, which consist of carrier gas plus the vaporized organic materials of the sample being analyzed, are mixed with H_2 and burned in a stationary diffusion flame whose combustion is supported by a continuous flow of air. As in the case of the E.C.D., a pair of electrodes is used to remove ions and free electrons from the ionization zone (viz. the flame). The bias electrode in Figure 9 is the burner jet, which is electrically biased, and the collector, which is connected to a current measuring device.

The chemi-ionization of hydrocarbons by the reaction $CH + O \rightarrow CHO^+ + e^-$ has been documented by Calcote (12) and Sugden (13) and is recognized as the mechanism for ion production in the F.I.D. (14). The H_2 flame itself produces no ions. The addi-

tion of trace amounts of hydrocarbon material, however, results in the production of ions at a rate that is proportional to the combustion rate of the organic material. In the ideal F. I. D. the electrode system removes all of the electric charge that is produced in the flame so that the detector response is proportional to the hydrocarbon combustion rate. Hence the classification, "linear mass rate detector".

Real flame ionization detectors, however, are not quite the ideal linear detector, although they come remarkably close to this goal. In order to study the mechanisms by which ions are produced and collected or lost and the way in which these mechanisms relate to F.I.D. operating characteristics, the conventional detector was modified to extremes in some of the experiments described in the following sections.

Flame Height Studies

An appropriate starting point for the study of F.I.D. response characteristics and design principles is an investigation of some of the physical properties of diffusion flames. One of the most frequently referenced papers on this subject is a report by Burke and Schumann (15) who analyzed the case of a flame burning on a cylindrical fuel jet on the axis of a larger cylindrical air conduit. The fuel jet wall was assumed to be negligibly thin and the flow of gases was postulated as laminar. The mixing of fuel and O_2 in this model is due solely to the inter-diffusion of the two gases. For sufficiently tall flames the mathematical analysis can be confined to the solution of the equation for radial diffusion. Combustion is limited to the flame front which is defined as the surface where fuel and O_2 meet and burn in a stoichiometric ratio. O_2 does not penetrate this surface nor does fuel diffuse outwardly beyond it. Combustion products, however, are free to diffuse in both radial directions from their origin at the flame front.

With the following notation:

z = distance above fuel jet

$\dot{z}$ = linear gas velocity parallel to the flame axis

R_o = inner radius of air conduit

r_o = radius of fuel jet

r = radial distance

k = coefficient of inter-diffusion

p_f = partial pressure of fuel in unburnt jet gases

p_o = partial pressure of O_2 in air supply

p = partial pressure of fuel at any point in space

i = number of moles O_2 required for complete combustion of one mole fuel

$P = p_f + p_o / i$

t = time

the equation for radial diffusion in cylindrical coordinates can be written:

$$\frac{\partial p}{\partial z} = \frac{k}{\dot{z}} \left[\frac{\partial^2 p}{\partial r^2} + \frac{1}{r} \frac{\partial p}{\partial r} \right] \qquad (21)$$

where $\partial (z/\dot{z})$ has been substituted for ∂t in the usual diffusion equation. Initial conditions are:

$$p = p_f, \; z = o \text{ and } o \leq r < r_o$$

$$p = -p_o/i, \; z = o \text{ and } r_o < r \leq R_o$$

where the latter condition was introduced by Burke and Schumann to surmount the difficulties presented by the fact that one boundary condition is $p = o$ at the flame front but until equation (21) is solved the coordinates of the flame front are unknown. Other boundary conditions are:

$$\partial p / \partial r = o \quad \text{at } r = o, R_o$$

The solution to equation (21) which satisfies the given conditions is, according to the authors

$$p = P (r_o/R_o)^2 - p_o/i + \frac{2 r_o}{R_o^2} P \sum \frac{J_1(ur_o) J_o (ur)}{u (J_o (uR_o))^2} \exp (-ku^2 z/\dot{z}), \qquad (22)$$

where J_o and J_1 are Bessel functions of the first kind and where u takes on all values which satisfy the equation $J_1 (uR_o) = o$ The summation in equation (22) is over all these values of u.

To solve for the coordinates of the flame front one has to solve equation (22) with p = o, which requires a graphical solution. However, examination of the exponential factor reveals two facts of interest to the scientist or engineer working with diffusion flames. Note that, in general, the value for p in equation (22) is unaffected by variations in k, z, and $\dot{z}$ which leave the quantity $kz/\dot{z}$ unchanged. Therefore, the flame height, which corresponds to z when p = o and r = o, is: (1) proportional to the linear gas velocity, $\dot{z}$, and (2) inversely proportional to the coefficient of inter-diffusion, k.

To explore the implications of the Burke and Schumann interpretation further, a computer program for the solution of equation (22) was written. As we will see later, the solution is also useful in describing the distribution of ions due to ambipolar diffusion inside a cylindrical tube whose inner surface represents an absorbing barrier. Details of the computer program are given in Appendix I. One of the results of this analysis, obtained for the special case, p = o, r = o, is shown in Figure 10 where we see a relationship between $kz/\dot{z}$ and the ratio of unburnt fuel to oxygen at the base of the flame. p = o, r = o corresponds to the top of the flame so that, if k and $\dot{z}$ are known, Figure 10 can be used to find the flame height z as a function of the partial pressure of fuel in the jet gases, the partial pressure of O_2 in the air supply and i, the stoichiometric ratio of O_2 to fuel for complete combustion. While the Burke and Schumann report has been succeeded by more complete analyses, such as that by Fay (16) which takes into account the conservations of mass and energy in the flame, Figure 10 is at least useful for a qualitative analysis of some of the physical aspects of diffusion flames. For example, lowering the value of p_f by diluting the fuel with an inert gas will result in a shorter flame while diluting the O_2 in the air supply will have the opposite effect. Note also that a partial pressure of 1 atm. for H_2 (i = 1/2) is equivalent in terms of flame height to a partial pressure of 0.25 atm. for CH_4 (i = 2).

When a hydrocarbon that has eluted from a GC column enters the diffusion flame of a F.I.D. the flame will increase in height for two reasons. First, even if

the value of i for a hydrocarbon is 1/2 (i.e. the same as for H_2), the flame will get larger due to an increase in p_f. That is, some of the carrier gas, which normally dilutes the H_2, will be displaced by the hydrocarbon (more fuel). Second, the value of i for hydrocarbons is generally greater than 1/2 so that the additional fuel will produce an increase in flame height that is larger than that which would be produced by the same partial pressure of H_2. These effects are most noticeable during the elution of solvent peaks. As the hydrocarbon burning rate increases, reaches a maximum, and finally decreases, the flame height will go through an analogous sequence, as can be verified by visual observation. The importance of this fact, as regards F.I.D. design, is that the proximity of collector electrode to flame must allow for the change in flame size with p_f and i. The following experiment demonstrates this.

Flame Height Experiment

A stainless steel capillary tube burner jet with I.D. = 0.038 cm. and O.D. = 0.0635 cm. was installed on the axis of a glass air conduit with I.D. = 0.4 cm. The unburnt jet gases consisted of 0.59 cm^3/sec H_2 + 0.242 cm^3/sec N_2 which were burned in a 234 cm^3/sec. air stream. By holding a ruler behind the glass tube, the flame height could be measured as 0.5 microliters of benzene eluted from a G.C. column. In a dark room the flame became visible at a height of approximately 0.05 cm and attained a maximum height of 0.35 cm. The flame was visible for approximately 5 seconds.

Bearing in mind the fact that the ideal conditions postulated in the Burke and Schumann analysis were not fully realized, let us compare the above experimental results to the theoretical predictions. For the jet gas flow rates and jet diameter used in this experiment, the average linear gas velocity at 293^{o}K is 730 cm^3/sec. The partial pressure of unburnt fuel is $p_f = 0.59 / (0.59 + 0.242) = 0.71$ atm. The partial pressure of O_2 in air is $p_{O_2} = 0.21$ atm. Since a half mole of oxygen is required for complete combustion of one mole of H_2, we have i = 0.5. Therefore,

$$i\,(p_f/p_{O_2}) = 1.775 \qquad (23)$$

The corresponding value for $kz/\dot{z}$ in Figure (10) is 1.87×10^{-4} cm^2 so that the flame height can be expressed as

$$z = 1.87 \times 10^{-4}\ \dot{z}/k \qquad (24)$$

Note that the temperature dependence of $\dot{z}$ (viz $\dot{z} \sim T$) is partially cancelled by the increase in diffusion rate with T. According to Gaydon and Wolfhard (17), k is proportional to the 1.75 power of the temperature. These authors also show a calculated temperature of 2373^{o}K for stoichiometric combustion of hydrogen and air in a pre-mixed adiabatic flame. Since the small FID diffusion flame does lose heat to its surroundings and since the average temperature of a diffusion flame is considerably less than its maximum value, let us take about one-half the adiabatic temperature, or 1200^{o}K, as an appropriate "first guess" temperature for estimating the value of k. At 273^{o}K the diffusion coefficient for H_2 in air is 0.611 cm^2/sec (18). Using the 1.75 power relationship suggested by Gaydon and Wolfhard, we get:

$$k = 0.611\ (1200/273)^{1.75} = 8.2\ \text{cm}^2/\text{sec} \qquad (25)$$

Equation (24) can now be used to compute a value for the flame height:

$$z = 1.87 \times 10^{-4}\ (730/8.2) \times (1200/293) = 0.068\ \text{cm}$$

where the factor (1200/293) is the temperature correction to the gas velocity whose value of 730 cm/sec corresponds to a room temperature of 293^{o}K. The calculated value of 0.068 cm for the height of the H_2 diffusion flame is in good agreement with the approximate height of 0.05 cm at which the flame first became visible after the addition of benzene. That is, the agreement is good in view of a possible 50% error in the flame height measurement and the crude method used for choosing an appropriate flame temperature for the calculations.

To compute the maximum flame height we must first estimate the partial pressure of fuel in the unburnt gases when the burning rate of benzene is at its maximum. The density of benzene at 20^{o}C is 0.879 gm cm^{-3} and its mole weight is

78.11 gms. Therefore, a 0.5 microliter injection of C_6H_6 at room temperature is equivalent to 5.62 micromoles. For the purpose of estimating the maximum partial pressure of C_6H_6, let us assume that the partial pressure rises linearly at a rate of A atm./sec for the first 2.5 seconds and then decreases at the same rate for the next 2.5 seconds. That is:

$$p_{c_6} = At, \quad o \leq t \leq 2.5 \text{ sec} \tag{26a}$$

$$= A(5-t), \quad 2.5 \leq t \leq 5 \text{ sec} \tag{26b}$$

$$= o, \text{ otherwise} \tag{26c}$$

The rate at which benzene is introduced into the flame can be expressed by

$$\dot{m} = QC, \tag{27}$$

where $\dot{m}$ is in moles of C_6H_6 per sec., Q is the volume flow rate of gas through the jet (a constant), and C is the concentration of unburnt benzene in moles per cm^3. That is,

$$C = p_{c_6} / RT, \tag{28}$$

where the ideal gas law has been used. Since 50% of the total injection burns during the first 2.5 seconds, we can write

$$\frac{M}{2} = \int_o^{2.5} \dot{m}\, dt = \frac{Q}{RT} \int_o^{2.5} p_{c_6}\, dt = \frac{QA}{RT} \int_o^{2.5} t\, dt \tag{29}$$

Solving equation (29) for A, we get

$$A = \frac{2RTM}{2Q(2.5)^2} = 2.6 \times 10^{-2} \text{ atm./sec} \tag{30}$$

where we have used:

$M = 5.62 \times 10^{-6}$ moles

$R = 82.06$ atm. cm^3 per mole per ^oK

$T = 293^oK$

$Q = (0.59\ H_2 + 0.242\ N_2)\ cm^3/sec = 0.832\ cm^3/sec$

Returning to equation (26a), we see that the maximum partial pressure occurs at

t = 2.5 sec and is equal to:

$$(p_{c_6})_{max} = 6.5 \times 10^{-2} \text{ atm.} \tag{31}$$

The Burke and Schumann model can now be used to compute the maximum flame height.

The complete combustion of one mole of benzene,

$$C_6H_6 + 7.5\ O_2 \rightarrow 6\ CO_2 + 3\ H_2O \tag{32}$$

requires 7.5 moles of O_2. Therefore,

$$i\,(p_{c_6})_{max} / p\,(O_2) = 7.5 \times 6.5 \times 10^{-2}/0.21 = 2.32 \tag{33}$$

The corresponding value for $kz/\dot{z}$ in Figure 10 is 2.42×10^{-4} cm^2. The coefficient for the inter-diffusion of benzene in air at 273^{o}K is 0.077 cm^2/sec. (18). At 1200^{o}K we have:

$$k = 0.077\ (1200/273)^{1.75} = 1.03 \text{ cm}^2/\text{sec.} \tag{34}$$

The flame height is given, therefore, by:

$$\begin{aligned} z &= 2.42 \times 10^{-4}\ \dot{z}/k \\ &= 2.42 \times 10^{-4} \times (730 \times 1200/293)/1.03 \\ z &= 0.70 \text{ cm} \end{aligned} \tag{35}$$

which is twice the observed maximum height. Better agreement between the observed and calculated flame heights can be obtained by assuming a higher flame temperature in the calculations of $\dot{z}$ and k ($\dot{z}/k \sim T^{-0.75}$). However, the significant result is that a solvent peak eluting from a GC column (1/2 microliter C_6H_6 is a representative example) causes the flame height to increase by approximately an order of magnitude. This is the conclusion of both the experimental observations and the theoretical analysis. Flame Ionization Detectors should, therefore, be designed for flames of variable size.

Inadequate Electrode Spacing

To study the kind of problem that can result from a detector design that does not allow for changes in flame size, the following experiment was performed:

A spherical platinum collector electrode with diameter = 0.2 cm was placed on the flame axis 1.9 cm above the capillary burner jet. The glass air conduit, capillary burner and platinum collector electrode of the previous experiment were assembled in a Varian Aerograph Model 1200 Chromatograph detector tower, as shown in Figure 11. The inner surface of the tower was lined first with Teflon for electrical insulation and then with a 0.012 cm thick aluminum foil insert, which served as the bias electrode. Figure 12 shows two sets of chromatograms due to 0.5 microliters of benzene obtained with this detector. The upper pair of chromatograms were obtained with the aluminum foil biased positively at 300 volts while the lower chromatogram was obtained with a foil potential of -300 volts. Note the double headed peaks that are especially prominent in the case of the positive foil and the dip above baseline that occurs before and after the major portion of the lower peak (negative foil). The positive vertical axis in Figure 12 corresponds to positive collector current which is to say collection of positive ions and/or emission of electrons from the platinum sphere. The negative half of the vertical axis corresponds to collection of negatively charged particles (viz. ions and/or free electrons) from the flame gases. The width, at baseline, of the lower peak is approximately 5 seconds, which corresponds to the time interval during which the flame was visible. The upper peaks are considerably broader.

If we assign the same time dependence to the flame temperature that was assumed as an approximation to the C_6H_6 burning rate in the flame height calculations, we can show that the maximum temperature of the collector electrode lags behind the flame temperature by 1.6 seconds. Since 1.6 seconds correlates with the time separation of the two heads of the upper peaks to within a factor of 3 or 4, it seems reasonable to assume that the splitting of the C_6H_6 chromatograms into two heads is

due to the chemi-ionization of the hydrocarbon (first head) followed by a thermal effect (second head). The difference between the positive and negative foil peaks suggests thermionic emission as the "thermal effect" although this hypothesis runs into difficulty as we will see in the following analysis.

The Hot Electrode

Consider the problem of heat transfer to a sphere in a stream of hot air. Since the coefficient of thermal conductivity is approximately three orders of magnitude greater for platinum than for air, we can assume that the rate of heat flow into the platinum is limited by the conductivity of the air film at the surface of the sphere and that the temperature gradients inside the sphere are negligible. The quantity of heat, dQ, that flows into the sphere in the time interval, dt, can be expressed as

$$dQ = Ah\,(T_g - T)\,dt, \qquad (36)$$

where A is the area of the sphere whose temperature is T, T_g is the temperature of the gases outside the surface film around the sphere (i.e., the temperature of the hot air stream), and h is the surface coefficient of heat transfer. The heat input, dQ, produces an increase in sphere temperature, dT, according to the relation

$$dT = dQ/VC\rho \qquad (37)$$

where V is the sphere volume and ρ and C are the density and specific heat of platinum respectively. Substituting $VC\rho\,dT$ for dQ in equation (36) and rearranging terms we get

$$dT = (A\,h/CV\rho)\,(T_g - T)\,dt \qquad (38)$$

For a sphere with diameter = 0.2 cm we have A/V = 30 cm. For platinum C = 0.0322 cal $gm^{-1}\,{}^{o}c^{-1}$ and ρ = 21.45 gm cm^{-3}. As shown by McAdams (19), the dimensionless variables $X \equiv DG/u$ and $Y \equiv hD/k$ are related according to the equation $Y = 0.37\,x^{0.6}$, where k and u are the thermal conductivity and viscosity of air

respectively, G is the fluid (air) flux in units of mass area^{-1} time^{-1}, and D is the diameter of the sphere. Therefore, we can express the surface coefficient of heat transfer, h, in the following way:

$$h = 0.37\ (k / D)\ (D\ G / u)^{0.6} \tag{39}$$

The air flow in this experiment was 23 cm^3 sec^{-1}, measured at room temperature and pressure. The density of air at 300^{o}K is 1.3×10^{-3} gm cm^{-3}. The inner diameter of the air conduit was 0.4 cm. The fluid flux, therefore, was

$$G = \frac{23 \times 1.3 \times 10^{-3}}{\pi\ (0.4/2)^2} = 0.238 \text{ gm cm}^{-2} \text{ sec}^{-1} \tag{40}$$

Using the data tabulated in the text by McAdams (19) one can show

$$u = 4.56 \times 10^{-6}\ T^{0.655} \text{ poise} \tag{41}$$

$$k = 1.04 \times 10^{-6}\ T^{0.73} \text{ cal cm}^{-2}\ (^{o}\text{K} / \text{cm})^{-1} \tag{42}$$

Substituting the expressions for u, and k and the values of D and G in equation (39), we get

$$h = 4.96 \times 10^{-4}\ T^{0.337} \tag{43}$$

Returning to equation (38) we note that the temperature dependencies of V and ρ cancel. An examination of the specific heat and coefficient of linear thermal expansion for platinum (e.g. see Handbook of Chemistry and Physics (20)) shows that the former changes by roughly 0.02% per ^{o}C and the latter is equal to 9×10^{-6}. Therefore, if we write

$$B \equiv A\ h / CV\rho \tag{44}$$

then

$$(1/B)\ dB/dT = (1/h)\ dh/dT + (1/A)\ dA/dT - (1/C)\ dC/dT \tag{45}$$

which for $T \gtrapprox 10^3\ ^{o}$K becomes

$$(1/B)\ dB/dT \gtrapprox 0.02\% \text{ per } ^{o}\text{K} \tag{46}$$

In other words, the quantity $B = Ah/CV\rho$ varies rather slowly with temperature so that it can be treated as an approximate constant in solving equation (38).

The gas temperature, T_g, will change with time as the benzene peak elutes from the column into the flame. Let us assume that T_g increases linearly with time for the first 2.5 seconds and then decreases at the same rate for the next 2.5 seconds. That is,

$$T_g = a + T_o + b\,t, \tag{47}$$

where T_o is the temperature of the gases above the flame when H_2 is the only fuel (i.e., before and after the benzene elutes) and

Case 1: $a = o$

$$b = (T_{max} - T_o) / 2.5, \quad o \leq t < 2.5 \text{ sec} \tag{48}$$

Case 2: $a = 2\,(T_{max} - T_o)$

$$b = -(T_{max} - T_o) / 2.5, \quad 2.5 \leq t < 5 \text{ sec} \tag{49}$$

Case 3: $a = b = o$, otherwise, (50)

where T_{max} is the maximum temperature of the gas. Substituting the general expression for T_g in equation (38), we get

$$dT = (A\,h/\,CV\rho)\,(a + T_o + b\,t - T)\,dt \tag{51}$$

which can be solved by substituting a temporary variable, x, for the quantity $a + T_o + b\,t - T$ and separating the variables x and T. The solution of equation (51) is

$$T - T_o = a + bt - \frac{1}{B}\left\{ b + \left[B(a + T_o + bt_i - T_i) - b \right] \exp\left(-B \left[t - t_i \right] \right) \right\} \tag{52}$$

where $B = Ah/CV\rho$, and T_i is the platinum sphere temperature at $t = t_i$. We now consider the three cases.

Case 1: $t_i = o$, $T_i = T_o$

$$T-T_o = (T_{max} - T_o) / 2.5 \left\{ t - \frac{1}{B} \left(1 - \exp \left[-Bt\right] \right) \right\} \quad (53)$$

Case 2: $t_i = 2.5$

T_i = sphere temperature at t = 2.5 seconds in case 1.

$$T-T_o = (5-t)\,(T_{max} - T_o) / 2.5 + \frac{1}{B} \left\{ \left(\frac{T_{max} - T_o}{2.5} \right) - \left(B \left[T_{max} - T_i \right] + \frac{T_{max.} - T_o}{2.5} \right) \exp \left(-B \left[t-2.5 \right] \right) \right\} \quad (54)$$

Case 3: $t_i = 5$

T_i = sphere temperature at t = 5 seconds in case 2.

$$T-T_o = (T_i - T_o) \exp \left(-B \left[t - 5 \right] \right) \quad (55)$$

Using the values for C, ρ, and A/V as stated earlier and the value for h at $T = 10^3\ ^oK$, as obtained from equation (43), we get, $B = 4.55\ sec^{-1}$. Equations (53), (54), and (55) can now be used to compute and plot the ratio, $(T - T_o) / (T_{max} - T_o)$ versus time, as shown in Figure 13.

The significant feature of Figure 13 is that the platinum sphere collector electrode attains its maximum temperature 1.6 seconds after the maximum in the air temperature. In the search for an appropriate thermal mechanism to account for the chromatograms shown in Figure 12, thermionic emission is an attractive candidate for the following reasons. In the case of the positive foil chromatograms the electrode polarity is such that the current which results from the thermionic emission of negative electrons out of the hot sphere has the same sense (or sign) as the positive ion current flowing into the sphere. Hence the relatively slow cooling of the platinum sphere, as shown in Figure 13 for t > 4 seconds, can account for the tailing of the positive foil chromatograms. In the case of the negative foil chromatogram, however, thermal electrons are emitted against the external electric field so that the slow cooling of

the sphere results in a dip above the baseline of the lower chromatogram in Figure 12. The sharp dip above baseline that occurs at the leading edge of the negative foil chromatogram cannot be explained in terms of thermionic emission and is not understood at this time.

To pursue the question of thermionic emission further, the height of the "thermal head" can be used with Richardson's equation to estimate the temperature that would be necessary to account for the data. Richardson's equation can be written

$$j = k_1 T^2 \exp(-k_2 / T), \qquad (56)$$

where j is the density of electron current emitted from the hot sphere in amp. cm^{-2} and T is the absolute temperature of the sphere. For platinum $k_1 = 1.7 \times 10^4$ amp $cm^{-2}\ {}^oK^{-2}$ and $k_2 = 7.25 \times 10^4\ {}^oK$ (see, for example, Cobine (5)). An examination of the positive foil chromatograms in Figure 12 shows that the amplitude of the second head is of the order of 10^{-8} amp. Since the area of a 0.2 cm sphere is 0.125 cm^2, the required current density is

$$j = \text{current/area} = 8 \times 10^{-8} \text{ amp } cm^{-2} \qquad (57)$$

which occurs when platinum is at a temperature of about 1770^oK. Returning to Figure 13 we note that the maximum platinum sphere value for $(T - T_o) / (T_{max} - T_o)$ is only equal to 0.36. In other words

$$T_{max}\ (\text{sphere}) = 0.36 \left[T_{max}\ (\text{gas}) - T_o\right] + To \qquad (58)$$

so that if T_o were as high as 1400^oK, the maximum gas temperature would have to equal 2235^oK. Subsequent measurement of the gas temperature at the fuel jet (i.e. at $z \approx o$) with a chromel-alumel thermocouple, however, produced a value of only 830^oC. While this value is undoubtedly low due to the thermal conductivity of the thermocouple, the temperature of the platinum sphere should have been affected in a similar manner by conduction to the brass screw from which it was suspended (See Figure 11).

Discussion of Thermal Effects

The application of Richardson's equation to the present problem is naive, since thermionic emission from platinum in a gaseous atmosphere requires a different value for the effective work function than that which is implicit in the value for k_2. The interaction of gas molecules with hot filaments has been analyzed and exploited for the measurement of electron affinities by Page (21). However, in the present case an alternate explanation seems more likely. The platinum sphere was formed on a 0.015" diameter Pt. wire which was suspended from a brass screw. At the point of suspension a flexible copper wire was soldered for the purpose of making an electrical connection to the current measuring device. The junction of the platinum and copper wires formed a thermocouple. Figure 14 is an equivalent circuit of the flame, thermocouple and operational amplifier which held the copper wire at (virtual) ground. The direction of the thermocouple E.M.F. is consistent with the effects observed in the chromatograms. That is, the increase in E.M.F., produced by an increase in temperature, generated a current whose direction was equivalent to the emission of electrons from the platinum sphere. The temperature of the thermocouple junction would be expected to lag behind the sphere temperature in time, since some of the heat responsible for raising the junction temperature would have to be conducted from the sphere through the platinum wire. This explains why the separation of the two heads in the benzene chromatogram was greater than that calculated for Figure 13. Unfortunately, a quantitative analysis of this interpretation was not possible without a reasonable estimation of the effective resistance of the gases.

Excessive Electrode Spacing

The anomalous double headed solvent peaks described in the previous sections were attributed to inadequate spacing between the flame and the collector electrode. This conclusion raises two questions: what is an adequate spacing and what happens when the spacing is excessive? To continue the investigation into the relation between detector characteristics and flame-electrode spacing, the detector shown in Figure 15 was constructed. The burner jet consisted of a 7.6 cm long stainless steel capillary

tube, with outer diameter = 0.089 cm and inner diameter = 0.051 cm, concentric with and enclosed by one of four brass tubes whose inner diameter was 0.6 cm and which directed the air flow from a standard Aerograph Model 1200 detector base to various heights above the flame. At an operating air flow rate of 61.3 cm^3/sec the flame burned in a laminar flow gas stream. A spherical platinum collector electrode housed in Teflon was mounted on one of the brass tubes at distances of 9.5, 22.2, 34.9, and 47.6 cm from the burner jet, depending on which of the four tubes was used.

The objective of this experiment was to measure the changes in the height and width of chromatographic peaks as the flame-to-collector electrode distance was varied. The following theoretical analysis, which is limited to ions in a laminar flow gas stream, explains the relationships between GC peak characteristics and the ion loss mechanisms of diffusion and recombination.

Recombination Theory

Let z denote the distance downstream from the flame along the axis of the brass tube in Figure 15. Suppose the spatial average ion density at z = o (i.e., in the flame) is a Gaussian function of time. That is

$$n_o(t) = N_o \exp\left(-(t-t_r)^2 / 2\sigma^2\right) \qquad (59)$$

where n_o = ion density at z = o

t = time

t_r = retention time of GC peak

σ = standard deviation of Gaussian peak (i.e., the peak width at 60. % peak height)

N_o = maximum ion density, which occurs at $t = t_r$

Assuming a laminar flow condition for gases inside the air conduit and neglecting radial diffusion for the time being, the ions that are produced in the flame will flow downstream through an imaginary pipe whose diameter is equal to that of the flame. If the flame

diameter is small in comparison to the inner diameter of the air conduit, the linear velocity of the ions along the conduit axis will be twice the average linear gas velocity. The latter is a well known consequence of the parabolic velocity profile for gases in laminar flow through circular pipes. If we denote the velocity along the axis by $\dot{z}$, the transit time required for ions to flow from the flame to the collector electrode is $z/\dot{z}$, where z is the distance between the flame and the electrode. Assuming that the densities of positive and negative ions in the flame are both equal to n_o, the rate at which the ion density above the flame changes with respect to the transit time, $z/\dot{z}$, is given by

$$dn/d\,(z/\dot{z}) = -\,an^2, \qquad (60)$$

where n is the density of ions at a height z when the linear gas velocity is $\dot{z}$ and $\underline{a}$ is the recombination coefficient. Integrating equation (60) with respect to $z/\dot{z}$, we get

$$n = n_o / (1 + a n_o\, z/\dot{z}) \qquad (61)$$

By hypothesis, n_o is a Gaussian function of time. Combining equations (59) and (61), the ion density in the neighborhood of the collector electrode can be expressed as a function of t and z,

$$n\,(z,t') = \frac{N_o \exp\left[-(t-t_r)^2 / 2\sigma^2\right]}{1 + N_o\, a\,(z/\dot{z}) \exp\left[-(t-t_r)^2 / 2\sigma^2\right]} \qquad (62)$$

where $t' = t + z/\dot{z}$.

Neglecting space charge effects, the collector current, I, will be proportional to the ion density, n. We can write, therefore

$$I = \frac{A \exp(-x^2)}{1 + B\,(z/\dot{z}) \exp(-x^2)} \qquad (63)$$

where A is a constant proportional to N_o

$$B = N_o\, a$$

$$x^2 = (t-t_r)^2 / 2\sigma^2$$

A plot of I versus x represents the chromatogram that would be obtained with a detector whose collector electrode is z cm downstream from the flame and when the linear gas velocity along the axis of the air conduit is $\dot{z}$ cm/sec.

One of the significant features of equation (63) is that it describes a chromatogram that becomes progressively less Gaussian-like as the value of $Bz/\dot{z}$ increases. This peak shape distortion arises from the fact that the rate of ion loss by recombination is proportional to the square of the ion density and hence is a non-linear effect. Consequently the dependence of B on N_o implies a detector response roll-off at high sample concentrations. To see this more clearly, consider equation (63) with x = o.

$$I_o = \frac{A}{1 + B\,z\,/\,\dot{z}} \qquad (64)$$

where we have introduced the subscript zero to denote the height of the chromatographic peak. A and B are both proportional to N_o. When N_o is sufficiently small we can write

$$B\,z/\dot{z} << 1$$

and

$$I_o \approx A \backsim N_o$$

In other words, if we assume that the ion density in the flame is proportional to the partial pressure of hydrocarbon in the unburnt gases, then the detector depicted in Figure 15 should have a linear response to injected samples that are sufficiently small. Roll-off, on the other hand, begins when $B\,z/\dot{z}$ approaches unity.

Since chromatograms often contain many peaks, it is desirable to minimize the detector's contribution to peak width for optimum resolution. To calculate the width at half height we use equation (63) to solve for x when $I = 1/2\ I_o$.

$$\frac{A \exp\,(-x_1^2)}{1 + B\,(z/\dot{z}) \exp\,(-x_1^2)} = \frac{A\,/\,2}{1 + B\,z/\dot{z}}$$

$$x_1 = \sqrt{\ln\,(2 + B\,z/\dot{z})}$$

$$\text{but } x_1 = \pm\,(t_1 - t_r)\,/\sqrt{2}\ \sigma$$

and the width at half height, w, is given by

$$w = 2\left|\,t_1 - t_r\right|$$

Therefore,

$$w = 2\sigma\sqrt{2 \ln (2 + B\, z/\dot{z})} \qquad (65)$$

Note that as $B\, z/\dot{z}$ approaches zero, w approaches $2\sigma\sqrt{2 \ln 2}$, which is the half width of the original Gaussian chromatogram described in equation (59). Conversely, as $B\, z/\dot{z}$ approaches the order of unity, either because of an increase in B due to a high density of ions in the flame ($B \backsim N_o$) or because of an excessive ion transit time, $z/\dot{z}$, the peak will become broader.

Radial Diffusion Theory

We began the section on ion recombination by neglecting radial diffusion, which enabled us to assume that the ions were bounded by an imaginary pipe whose diameter was equal to that of the flame. We now neglect recombination and consider the fact that the ions are free to diffuse radially as they travel upward from the flame in a laminar flow gas stream. In the case of ambipolar diffusion in an unbounded volume it can be shown that

$$\bar{r}^2 = r_o^2 + 4\, k\, t \qquad (66)$$

where k is the diffusion coefficient and $4\,\bar{r}^2$ is the mean squared width of the radial ion distribution t seconds after the ions are produced in a flame whose diameter is $2\, r_o$. As long as the ions do not diffuse too far from the air conduit axis, the ions will travel a distance of approximately $z = \dot{z}\, t$ downstream from the flame in the time that it takes for the mean squared width to grow to $4\,\bar{r}^2$. In this case equation (66) can be re-written as a function of z and $\dot{z}$.

$$\bar{r}^2 = r_o^2 + 4\, k\, z/\dot{z} \qquad (67)$$

Note that the width of the ion density distribution z cm above the flame when the gas velocity is $\dot{z}$ is the same as the width at a height fz cm above the flame when the gas velocity is increased or reduced by a factor of f.

In the case of the present experiment the ions are diffusing toward the inner

surface of an air conduit that is electrically grounded and which represents an absorbing barrier. Furthermore, as the ions diffuse away from the flame axis, the linear velocity of the gas stream changes. For laminar flow through a circular pipe the linear gas velocity is a function of the radial distance, r

$$\dot{z}\,(r) = 2\,\dot{z}_o\,(1 - (r/R_o)^2), \qquad (68)$$

where $\dot{z}_o$ is the volume flow rate divided by the cross sectional area of the pipe whose inner radius is R_o. In the following analysis we will compute the radial ion density distributions inside the air pipe for the case of a uniform linear gas velocity after which the effects of the parabolic velocity profile, equation (68) will be considered.

To compute the radial ion density distributions we return to equation (22) of the Burke and Schumann analysis. Assuming that the ion density at z = o can be described approximately by:

$$p = n_o,\ o \leq r \leq r_o$$
$$p = o,\ r_o < r \leq R_o$$

the other appropriate boundary conditions, valid for all values of z, are

$$\partial n/\partial r = o,\ r = o,\ R_o$$

and $p = o$ at $r = R_o$

The computer program described in Appendix I was used with the following input data

$$\dot{z} = 434 \text{ cm/sec}$$
$$R_o = 0.3 \text{ cm}$$
$$r_o = 0.0455 \text{ cm}$$
$$k = 0.035 \text{ cm}^2/\text{sec}$$

$\dot{z} = 434$ cm/sec is the linear gas velocity along the axis of a 0.6 cm diameter pipe when the volume flow rate is 61.3 cm^3/sec and r_o is one-half the outer diameter of the

capillary burner jet. In view of the fact that the capillary tube wall thickness was finite it was felt that the outer diameter was a more realistic approximation to the flame width than the inner diameter. k is the coefficient for the inter-diffusion of ions in air. The value, 0.035 cm^2/sec, is the average of the coefficients for positive and negative ions in air shown by Cobine (5) who quotes the work of J. J. Thomson and G. P. Thomson. The results of these computations are shown in Figure 16 where we see radial distributions for the relative ion density, n/n_o, at various heights above the flame. As in the case of ambipolar diffusion without absorbing barriers, the values of z can be scaled for gas velocities other than 434 cm/sec. That is, if the gas velocity were reduced to 217 cm/sec the density distribution labeled z = 22.22 would pertain to a height, z = 11.11 cm.

The density distributions shown in Figure 16 can be used to calculate the fraction of flame ions that reaches the collector electrode, under the hypothesis that collision with the air conduit is the only mechanism for ion loss in an air stream whose linear velocity is uniform across the diameter of the air conduit. The total number of ions, $\mathcal{N}$, in the volume element $dV = \pi R_o^2\, dz$ at a height z cm above the flame is given by

$$\mathcal{N}(z,t') = n_o(t)\, dz \int_o^{R_o} 2\pi r \frac{n}{n_o}(r,z)\, dr \qquad (69)$$

where $n_o(t)$ is the ion density in the flame (a function of time) and $\frac{n}{n_o}(r,z)$ are the density distributions shown in Figure 16. Assuming that the electrode system collects all ions which reach the height z, a plot of $\mathcal{N}$ versus t represents the chromatogram that would be obtained with the detector shown in Figure 15 under the present hypotheses. The relative ion density at z = o is given by

$$\frac{n}{n_o}(r,o) = 1, \quad 0 \leq r \leq r_o$$

$$= o, \quad r_o < r \leq R_o$$

Therefore, the number of ions in the volume element $\pi R_o^2\, dz$ at z = o is

$$\mathcal{N}(o,t) = n_o(t)\, dz\, \pi r_o^2 \qquad (70)$$

To compute the fraction, F, of these ions which survive long enough to reach the collector electrode z cm above the flame, we divide equation (69) by equation (70) to get

$$F(z, R_o) = (2/r_o^2) \int_o^{R_o} r \frac{n}{n_o}(r, z)\, dr \qquad (71)$$

Evaluation of the integral in equation (71) is facilitated by finding an analytical expression for n/n_o. Anticipating, from the appearance of the curves in Figure 16, that the density distributions are practically Gaussian, the computed values for n/n_o at $z = 47.62$ cm were plotted versus $(r/R_o)^2$ on semi-log graph paper as shown in Figure 17. The straight line segment in Figure 17 can be described by

$$\frac{n}{n_o}(r, 47.62) = 0.125 \exp(-5.35\, r^2/R_o^2) \qquad (72)$$

for $0 \leq r \leq 0.9\, R_o$. The boundary conditions in this analysis require that $n/n_o = o$ at $r = R_o$. However, if we substitute the expression in equation (72) for n/n_o in the integrand of equation (71) and integrate from 0 to $0.9\, R_o$ we get $F = 1$ to within slide rule accuracy. This means that the loss of ions due to diffusion to the inner surface of the air conduit at $z = 47.62$ cm is negligible. Since the ion density distributions in Figure 16 are more narrow for $z < 47.62$, the latter result implies that ion loss by diffusion is negligible for $0 \leq z \leq 47.62$ cm.

We now turn to the problem of the parabolic velocity profile and the bearing it has on the conclusions of the previous paragraph. Of the flame ions which reach the height z, a fraction $F(z, r_1)/F(z, R_o)$ is distributed in the interval $0 \leq r \leq r_1$, where r_1 is some radial distance less than R_o. For Gaussian density distributions,

$$n/n_o = A \exp(-B\,(r/R_o)^2),$$

where A and B are constants such that $F(z, R_o) = 1$, it can be shown (see Appendix II) that

$$F(z, r_1) / F(z, R_o) = F(z, r_1) = 1 - \exp(-B(r_1/R_o)^2) \qquad (73)$$

The average laminar flow velocity for particles whose radial coordinate falls in the

interval $0 \leq r \leq r_1$, is given by (see Appendix II)

$$\overline{\dot{z}}\,(r_1) = 2\,\dot{z}_o \left(1 + \left(\frac{(r_1/R_o)^2 + 1/B}{1 - \exp\left(-B\,(r_1/R_o)^2\right)}\right) \exp\left(-B\,(r_1/R_o)^2\right) - 1/B\right) \qquad (74)$$

The error incurred in the diffusion analysis, because of the parabolic velocity profile, is greatest for the broadest radial ion density distribution. That is, the density distribution at z = 47.62 cm represents the worst case. Inserting B = 5.35 and $r_1/R_o = 0.5$ into equation (73), we find that 73.8% of all the ions at z = 47.62 lie in the interval $0 \leq r \leq 0.5\ R_o$. Equation (74) can be used to show that the average linear velocity for these ions is 90.2% of the linear gas velocity along the axis of the air conduit. Therefore, approximately 3/4 of all the ions at z = 47.62 cm have an average linear velocity that differs from the value used in the diffusion analysis by only 10%. In view of the fact that the other density distributions are weighted more heavily at the z axis, the use of a uniform linear velocity equal to the gas velocity along axis of the air conduit appears to have been a good approximation in the diffusion analysis.

Theoretical Conclusions

The most significant difference between ion loss by recombination and the ion loss by collision with the air conduit is that the former produces both a reduction in peak height and an increase in peak width, while the latter merely results in an overall attenuation of the chromatogram. When recombination is the dominant mechanism for ion loss, equations (64) and (65) describe the peak height and width respectively as functions of the transit time, $z/\dot{z}$, and (implicitly) the maximum ion density in the flame, N_o. In the case of ion diffusion, however, we have the following situation. For $z \leq 47.62$ cm radial diffusion is confined to a distance less than 0.3 cm (i.e., the inner radius of the air conduit). If we assume that diffusion in the z direction causes the vertical distribution of ions to spread by as much as $\pm$ 0.3 cm, we find that the width of a chromatogram obtained with the collector electrode at z = 47.62 cm should increase by $0.6/\dot{z}$ seconds over the width measured at z = o. In the present analysis $\dot{z}$ = 434 cm/sec so that $0.6/\dot{z}$ = 1.4 m sec. Since the widths

of chromatographic peaks are of the order of 10 seconds or larger, 1.4 m sec. would produce an increase in peak width of 0.014% at most. This increase is not measurable with ordinary G.C. systems and can, therefore, be neglected in the present analysis. It has been shown that for $z \leq 47.62$ cm the ion loss due to diffusion alone is negligible. Therefore, diffusion can account for neither a reduction in peak height nor a change in peak width in the present analysis.

To generalize the conclusions of this analysis to larger values of z (or smaller values of $\dot{z}$) where ion loss to the air conduit becomes appreciable, consider equation (71) which describes the fraction of ions that reaches a height z. $F(z, R_o)$ is not a function of the ion density in the flame, or, to put it another way, the relative ion density distributions in Figure 16 are independent of the absolute ion density in the flame. Therefore, equation (71) implies that when ion loss by diffusion is appreciable every point on the chromatogram is lowered by the same factor, namely $F(z, R_o)$. In other words, the effect is the same as would occur if the gain on the chart recorder were reduced.

The effects of diffusion and recombination have been treated, so far, as independent mechanisms. The rate at which ions are lost by recombination is proportional to the square of the ion density, as shown in equation (60). As ions diffuse away from the z axis, they distribute themselves over a larger volume, which results in a lowering of their density and hence a reduction in the rate at which ions are lost via recombination. On the other hand, the rate at which gaseous particles diffuse in any given direction is proportional to the negative density gradient in that direction. Since the ion density distributions in Figure 16 are maximum on the z axis, the ions diffuse away from the axis. However, the loss of ions by recombination is greater on the z axis than it is for $r \neq o$. Therefore, the effect of recombination is to slow down the diffusion process (i.e., recombination tends to reduce the radial density gradient). Since the ion loss mechanisms of recombination and diffusion tend to slow each other down, the effects that either may have on chromatographic peak characteristics are weaker when both mechanisms act simultaneously than when each mechanism is

considered separately.

Experimental Investigation of Ion Losses

A hydrocarbon sample consisting of 8.5×10^{-7} gms hexadecane in 0.5 microliter benzene was separated on a 5-ft. x 1/8-in. stainless steel column packed with 3% SE 30 on 60-80 mesh Aeropak W at 185°C. The stainless steel capillary jet (See Figure 15) gases consisted of 0.5 cm^3/sec N_2 carrier gas + 0.5 cm^3/sec H_2. The total gas flow through the brass air conduit was 61.3 cm^3/sec, measured at ambient temperature and pressure. The gas flow was measured at the top of the air conduit while the flame was burning so that 61.3 cm^3/sec refers to the flow of air plus combustion products.

According to Gaydon and Wolfhard (17) the flow of gas through a tube is laminar when the Reynolds number, R_e, is less than 2300, where

$$R_e = 2 R_o \dot{z}_o / v$$

and where $2R_o$ is the diameter of the tube, $\dot{z}_o$ is the average linear gas velocity through the tube and v is the kinematic viscosity of the fluid in the tube. For air at 30°C we have

$$v = \text{viscosity/density}$$
$$= 1.7 \times 10^{-4} \text{ poise}/1.165 \times 10^{-3} \text{ gm cm}^{-3}$$

Since $2R_o = 0.6$ cm and $\dot{z}_o = 217$ cm/sec, the Reynolds number is

$$R_e = 900 < 2300$$

Therefore, the flow of gases through the air conduit should have been laminar. Furthermore the air had to flow through 7.6 cm of conduit before reaching the flame at the end of the capillary burner. 7.6 cm provided almost 13 air tube diameters for the laminar flow condition to become fully developed. The air flow had to be reduced temporarily during the combustion of the relatively large benzene solvent peak in order to prevent the flame from "lifting off" in the swift air stream.

Finally, the non-turbulent nature of the flame could be observed directly by looking down through the air conduit when the hexadecane eluted from the G.C. column.

Figure 18 is a plot of reciprocal peak height versus the computed transit time necessary for ions to travel to the collector electrode whose height above the flame was varied by using air tubes of different lengths. The point at $z/\dot{z}$ = 3 m sec corresponds to the chromatogram obtained with a standard F.I.D. whose collector electrode was a 0.6 cm diameter wire loop situated 1.9 cm above the top of an electrically insulated burner which was biased at -300 volts. The flame, therefore, was burning in an electric field of approximately 160 volts/cm. Since the mobility of flame ions is roughly 1 or 2 cm/sec per volt/cm (3), (17), the ion velocity in this case was equal to the gas velocity plus the drift velocity (i.e., an additional 200 cm/sec, or so).

The linear relation between $1/I_o$ and $z/\dot{z}$ that appears in Figure 18 is implicit in equation (64). From that equation we see that the intercept of the straight line in Figure 18 is equal to 1/A and the slope is equal to B/A. By definition B is equal to the product of the recombination coefficient, a, and the ion density in the flame, N_o, which corresponds to the hexadecane peak height (i.e., N_o is the ion density when the burning rate of C_{10} is maximum). We get, therefore,

$$B = \text{slope/intercept} = aN_o \tag{75}$$

From our knowledge of I_o, $\dot{z}$, and the flame diameter we can estimate the value of N_o.

$$I_o = (q N_o)\, \pi r_o^2\, \dot{z} \tag{76}$$

where q is the charge per ion so that $q N_o$ is the charge density in coulombs per cm^3 for ions of either sign. Solving for N_o, we get

$$N_o = 1.5 \times 10^9 \text{ ions/cm}^3$$

where we have used the intercept, 0.1×10^{10} amp^{-1}, in Figure 18 to obtain a value for

the peak height, I_o, that would be measured at the surface of the flame and where we have used

$$q = 1.6 \times 10^{-19} \text{ coulombs}$$

$r_o = 0.045$ cm, the outer radius of the capillary burner

$\dot{z} = 434$ cm/sec (gas velocity) +

200 cm/sec (drift velocity)

$= 634$ cm/sec

Using equation (75) and the data shown in Figure 18 we find

$$B = 130 \text{ sec}^{-1} = a N_o$$

$$a = B/N_o = 0.87 \times 10^{-7} \text{ cm}^3/\text{sec}$$

This value for the ion recombination coefficient is consistent with the approximate range, $10^{-7} < a < 10^{-6}$, for flame ions, as stated in the text by Gaydon and Wolfhard (17).

A linear relationship between $\exp(w^2/8\sigma^2)$ and the transit time $z/\dot{z}$ is implicit in equation (65). The latter equation implies

$$\exp(w^2/8\sigma^2) = 2 + B(z/\dot{z}) \qquad (77)$$

In Figure 19 we see that the experimental results substantiate equation (77). The value for σ, the width of the chromatogram at 60.7% of its full height, was obtained from the chromatgram at $z/\dot{z} = 3$ m sec. Strictly speaking, σ refers to the width of the chromatogram at $z/\dot{z} = o$. The 3 m sec error, however, is not significant, as can be seen by examining Figure 19. The slope of the line in Figure 19 yields a value of 66 sec^{-1} for B, which is less than the value obtained from the peak height data by about a factor of 2. This discrepancy is within experimental error. For example, if we delete the data points at $z/\dot{z} = 22$ and 51 m sec in Figure 18, the line which goes through the remaining three points yields a value of approximately 70 sec^{-1} for B.

Discussion of Experimental Results

The results of this experiment are consistent with the conclusions arrived at

in the theoretical analysis of ion loss by recombination and diffusion. The conclusion that recombination is the dominant mechanism for ion loss for $z \leq 47.62$ cm in the present experiment is verified by the peak width data shown in Figure 19. An error in the value used for the diffusion coefficient in the theoretical analysis could have resulted in a false estimate of the number of ions lost at the inner surface of the air conduit. However, it was shown that diffusion could account for only a 1.4 m sec increase in the width of a chromatographic peak. In order for ion diffusion to account for an additional Δt in the peak width, the ions would have to diffuse an extra $\Delta z = \pm \dot{z}\ \Delta t/2$ (i.e., Δz would cause the vertical ion distribution to arrive at the collector electrode $1/2\ \Delta t$ seconds earlier and to lag behind the original distribution by $1/2\ \Delta t$). For $\Delta t = 1$ sec and $\dot{z} = 434$ cm/sec we get $\Delta z = \pm 217$ cm. Equation (67) can be used to estimate the width of the vertical ion density distribution.

$$\overline{\Delta z^2} = \Delta z_o^2 + 2k\, z/\dot{z} \qquad (78)$$

where the factor 4 in the second term on the right hand side of equation (67) has been changed to a 2 because we are now dealing with a one-dimensional problem (see references 35 and 3, page 140). Differentiating equation (78) with respect to k we get

$$\frac{d\,\overline{\Delta z^2}}{dk} = 2\, z/\dot{z} \qquad (79)$$

The largest experimental value of $z/\dot{z}$ was 110×10^{-3} sec., which was the transit time for ions to reach a height of 42.67 cm. The change in diffusion coefficient, dk, necessary to produce the additional $\pm$ 217 cm spread in the vertical density distribution (i.e., to produce an additional 1 sec in the width of a chromatogram obtained at $z = 42.67$ cm) is

$$dk = (217)^2 / 2 \times 110 \times 10^{-3} = 3.3 \times 10^5 \text{ cm}^2/\text{sec}$$

Therefore, the data shown in Figure 19 must be due to the mechanism of ion recombination, as the mechanism of diffusion could only have a measurable effect on the widths of chromatographic peaks if k were of the order of 10^5 (i.e., if the fractional error in the value of k used in the theoretical analysis were of the order of 10^7).

The conclusion that ion recombination is the dominant mechanism for ion loss

in flame ionization detectors has interesting implications regarding detector theory and design principles. Let us assume, as the present results seem to substantiate, that equation (61) determines the F. I. D. 's response characteristics. If we assume that the detector current, I, is proportional to the ion density in the neighborhood of the collector electrode, n, and that the ion density in the flame, n_o, is proportional to the hydrocarbon combustion rate, $\dot{m}$, then equation (61) can be written

$$I = \frac{K \dot{m}}{1 + (C \ a \ z/\dot{z}) \dot{m}} \qquad (80)$$

where K and C are constants. Figure 20 shows response curves for four hypothetical detectors whose response, I, in amp is related to the combustion rate, $\dot{m}$, according to equation (80). The curves were computed for the case $K = 5 \times 10^{-3}$ coulombs/gm and for four different values of the parameter $B = C \ a \ z/\dot{z}$ $(gm/sec)^{-1}$. Note that for sufficiently small values of $\dot{m}$, such that $B \dot{m} << 1$, I is directly proportional to $\dot{m}$. The exact point at which response curve roll-off commences is a matter of arbitrary definition. However, it is clear that, from a practical point of view, the linear range of detector operation is extended as the value of B decreases. Since the parameter B is proportional to z, the recombination theory from which the curves in Figure 20 were derived implies an extension of the linear range with decreasing flame to electrode spacing. This conclusion is consistent with the experimental results of McWilliam (22), Ongkiehong (23) and Desty, Geach and Goldup (24). The parameter B is inversely proportional to $\dot{z}$, the velocity at which ions travel from the flame to the collector electrode. In a conventional detector $\dot{z}$ is the sum of the gas velocity and the ion drift velocity. The latter is proportional to the electric field set up by the collector and bias electrodes. For a given electrode spacing, the electric field is proportional to the voltage drop, V, across the electrodes. We can write, therefore,

$$B \backsim 1/\dot{z} = 1/(\dot{z}_g + kV) \qquad (81)$$

where $\dot{z}_g$ is the linear gas velocity and k is a constant related to the inter-electrode spacing. Therefore, as the bias potential is increased, B become smaller with the result that the linear range of detector operation is extended to higher values of $\dot{m}$.

This conclusion is consistent with the experimental results of Dewar (25) and Kaiser (26). It appears, therefore, that the roll-off in the F.I.D. response curve and its dependence on electrode spacing and bias potential can be explained qualitatively, at least, by ion recombination theory.

F. I. D. Response Roll-Off

In order to test the conclusions of the previous section beyond the fact that they are qualitatively correct, F. I. D. response data in the roll-off or "overload" region of operation were needed. The published results of McWilliams (22), Ongkiehong (23), Desty (24), Dewar (25) and Kaiser (26) contain insufficient detail for adequately testing the validity of equation (80). In general, the mechanism of ion recombination has been recognized as playing a role in response curve roll-off. Ongkiehong (23) in particular recognized the dependence of ion transit time on electrode spacing and bias potential and the relevance of transit time to response characteristics vis a vis the recombination equation. However, it appears that the only serious attempt that has been made to obtain enough data for precise analysis in the roll-off region is the work of Cohen, Parzen and Bailey (27). It is interesting to note that these authors attributed the overloading effect to a non-linearity in the ionization efficiency of the flame and not to losses by recombination. In other words, they concluded that the drop in the ratio of coulombs collected by the electrodes per gram of hydrocarbon burned in the flame was due to a drop in the number of coulombs produced in the flame. This, of course, contradicts the assumption made in formulating equation (80) where K is a constant.

The ionization efficiency interpretation of response curve roll-off cannot, by itself, explain the electrode spacing and voltage characteristics of F.I.D. operation. That is, if the detector's response drops off because there are fewer ions per gram of hydrocarbon available for collection, why does an increase in bias potential produce an increase in the quantity of charge collected? Ion multiplication by electron impact

in a stronger electric field would produce an increase in detector current in the linear range of operation as well as in the roll-off region. This, however, is not the case. An increase in voltage produces an extension of the linear range in the manner indicated in Figure 20 as B goes from 2530 to 506, for example.

An attempt was made to see if the published data of Cohen, Parzen and Bailey were consistent with the recombination model. The results of this effort were inconclusive. However, one of the difficulties encountered served to illustrate a more general problem that exists in the field of detector characteristics specification. The Cohen group measured, in effect, the total charge collected as a function of the total quantity of injected material. To use this data for testing the recombination model, both sides of equation (80) must be integrated with respect to time to obtain a relationship between the total collected charge and the total injected mass. The integration can be performed by assuming a suitable time dependence for $\dot{m}$ (e.g. let $\dot{m}$ be a Gaussian function of time). In general, the results of this integration will yield a relation between charge and mass that is different from the relation between the rate of charge collection, I, and the rate of mass combustion, $\dot{m}$. While this difference is only appreciable for detector operation in the roll-off region of response, it does present a problem when one attempts to compare the response characteristics of commercially available detectors.

F. I. D. Calibration Experiment

In view of the scarcity of published data in the overload region an experiment was performed with the detector shown in Figure 9. The objective of this experiment was to measure the instantaneous detector current, I, as a function of known hydrocarbon combustion rates, $\dot{m}$, in the overload region of response. An exponential dilution flask, similar to the one described by Lovelock (28), was used for generating ... ombustion rate whose time dependence could be established accurately. The exponential dilution flask (E.D.F.) is a glass mixing chamber. Normally, a gaseous sample of known quantity is injected into the chamber, by the use of a syringe, via a rubber septum in the inlet port. Carrier gas flowing through the inlet port transfers

the sample into the chamber where it is mixed by a magnetic stirrer to produce an initial concentration that can be determined if the flask volume is known. The concentration of this sample in the carrier gas that flows out of the chamber through the outlet port can be shown (28) to be an exponentially decaying function of time. That is,

$$p = p_o \exp(-Qt/V) \qquad (82)$$

where p is the partial pressure of the sample in the carrier gas as it leaves the flask, p_o is the initial partial pressure of the sample in the flask, Q is the volume flow rate of carrier gas through the flask and V is the flask volume. By plumbing the E.D.F. directly into the base of the F.I.D. a continuous I versus $\dot{m}$ response curve chromatogram can be obtained.

To satisfy the objectives of the present experiment the above procedure was attempted with $p_o = 1$ atm. That is, the flask was initially filled with butane which was then diluted with N_2 carrier gas, after the E.D.F. was valved into the detector base. It was found, however, that with an air supply of 6.67 cm^3/sec the detector flame could not be sustained. It was decided, therefore, to modify the dilution method so that the detector's response could be measured as the partial pressure of butane was increased from zero to whatever value caused the flame to go out. The outlet port of the E.D.F. was plumbed directly to the detector while the inlet port was connected to a switching valve. Initially pure N_2 carrier gas flowed through the flask and into the detector where it was mixed with H_2 and burned in an air supported diffusion flame. The valve was used to switch butane gas at a partial pressure of 1 atm. into the flask.

If p_f is the partial pressure of butane in the flask, then Vp_f is the total quantity of butane in the flask in cm^3 atm. The rate at which this quantity changes is equal to the difference between the rate at which butane gas is admitted into the flask and the rate at which butane leaves the flask in the diluted mixture.

$$d\,(Vp_f)dt = Qp_i - Qp_f$$

$$dp_f/dt = (Q/V)\,(1 - p_f) \qquad (83)$$

where we have made use of the fact that the flask volume, V, is a constant and the partial pressure of butane in the inlet port, p_i, is 1 atm. Integrating both sides of equation (83) with respect to time, we get

$$p_f = 1 - \exp\,(-Qt/V) \qquad (84)$$

where we have made use of the fact that $p_f = o$ at $t = o$. After measuring the gas flow rate and the flask volume, equation (84) can be used to transform a chromatogram (viz. the detector's response to the E.D.F. effluent) into a calibration curve by using the observed time dependence of I and the computed time dependence of p_f.

In detector calibration analyses large numbers of data points are desirable. Measuring the detector's instantaneous response from a strip chart recording is tedious and yields data whose resolution is limited by the strip chart recorder's plotting speed. A more sophisticated method for acquiring data was, therefore, devised. The Varian Aerograph Model 480 Digital Integrator is normally used for measuring the area under a chromatographic peak. However, it is possible to trigger the integrator at regular intervals so that it prints out the integrated detector response that has been accumulated in the interval between some start time and the n^{th} triggering. If Δt is the time interval between successive triggerings, the average detector current in the n^{th} interval is given by

$$I_{av} = (q_{n+1} - q_n)/\Delta t \qquad (85)$$

where q_{n+1} is the integrated response at $t = (n + 1)\Delta t$ and q_n is the integrated response at $t = n\,\Delta t$. By using the mean value theorem of calculus, it can be shown that I_{av} is equal to the instantaneous current for some value of t in the interval $(n + 1)\,\Delta t \leq t \leq n\,\Delta t$. Therefore, we can drop the subscript on I_{av} in equation (85) and treat I as the instantaneous current with the qualification that the integrator + triggering system has a time resolution of $\pm\ \Delta t/2$.

Figure 21 shows a schematic drawing of the F. I. D. calibration system. The triggering device consisted of a motor driven aluminum disk with four ridges milled into it and a micro-switch. The arrangement was such that the micro-switch was closed by the ridges four times per revolution which amounted to once every 1.137 seconds. The micro-switch was wired to the integrator so that a print command was initiated every time the circuit closed. A print frequency of 1 sec^{-1} appeared to be the upper limit for the printer.

The detector was operated with an air flow of 6.67 cm^3/sec and a hydrogen flow rate of 0.5 cm^3/sec. The N_2 flow rate through a 191.2 cm^3 E.D.F. was 0.221 cm^3/sec. About 700 data points were obtained as the partial pressure of butane in the E.D.F. effluent rose from zero to 0.6 atm in 15 minutes. Figure 22 shows the detector's response over this period, as plotted by a strip chart recorder which ran simultaneously with the integrator.

Interpretation of Calibration Results

The most interesting and unexpected outcome of this experiment was the fact that the chromatogram in Figure 22 has a maximum at a butane partial pressure of approximately 0.3 atm. This, of course, is not consistent with the recombination model which predicts that the chromatogram in Figure 22 should approach a limit asymptotically as p_f approaches 1 atm. In view of the flame extinction problem that had been encountered in the first E.D.F. experiment and the obvious loss in ionization efficiency for $p_f \gtrsim 0.3$ atm. in Figure 22, the Cohen, Parzen and Bailey interpretation was given further consideration.

A consideration of the mixing phenomenon in the E.D.F. and the internal geometry of the detector shown in Figure 9, suggests the following interpretation for F. I. D. response, the "O_2 depletion theory":

Let the flow rates of unburnt H_2, N_2, air and fuel (hydrocarbon) be denoted by a, b, c, and f respectively. Let F denote a normal hydrocarbon, $C_nH_{2(n+1)}$ so that for stoichiometric combustion we have

$$f\,F + \left(\frac{3n+1}{2}\right) f\,O_2 \rightarrow n\,f\,CO_2 + (n+1)\,f\,H_2O \qquad (86)$$

If we denote air by A, the combustion of H_2 and F (and N_2) in air can be written

$$aH_2+bN_2+cA+fF \rightarrow (b+0.8c)N_2+\left[a+(n+1)f\right]H_2O+nfCO_2+\left[0.2c-(3n+1)f/2-a/2\right]O_2 \qquad (87)$$

where we have made use of the fact that air is approximately 20% O_2 and 80% N_2, by volume, and where n is the number of carbon atoms in the normal hydrocarbon molecule.

Unburnt air and combustion products flow out from the detector through a small hole in the detector tower lid (see Figure 9). The internal volume of this detector is approximately 16 cm^3. If we think of the F.I.D. enclosure as a mixing chamber, it seems reasonable to assume that the flame burns in a mixture of air plus combustion products. The sketch in Figure 23 illustrates the mixing effect of the gas flow pattern that probably exists inside the detector tower. The time constant for this "mixing chamber" (i.e., detector volume/gas flow rate) is approximately 2 seconds for the operating flow rates stated earlier. If we assume perfect mixing, the partial pressure of O_2 inside the detector can be calculated. Let p'_{O_2} denote the ratio of the partial pressure of O_2 to the total gas pressure (viz. 1 atm.) inside the detector.

$$d\,(V_d p'_{O_2})/dt = 0.2c - Qp'_{O_2} - ((3n+1)\,f/2 + a/2) \qquad (88)$$

where V_d is the detector volume so that $V_d p'_{O_2}$ is the quantity of O_2 present inside the detector in cm^3 at 1 atm. The first term on the right-hand side of equation (88) is the rate at which O_2 enters the detector in the air input. Qp'_{O_2} is the rate at which O_2 flows out through the exhaust port, where Q is the flow rate out of the detector and which, in general, is not equal to the total flow rate into the detector. The last two terms are the rates at which O_2 is consumed by hydrocarbon and H_2 in the formation of H_2O and CO_2. If none of the terms on the right-hand side of equation (88) changes appreciably in a 2-second interval (i.e., the time constant for the detector) we can consider the "equilibrium" partial pressure of O_2 which can be calculated by equating the left-hand side of equation (88) to zero. We get

$$p'_{o_2} = \frac{0.2\,c - ((3n+1)\,f/2 + a/2)}{Q} \qquad (89)$$

Let p'_f denote the ratio of the partial pressure of unburnt hydrocarbon in the jet gases to the total pressure (viz. 1 atm.) of the jet gases.

$$p'_f = f/(a+b+f) \qquad (90)$$

Now, let us assume that the detector response is proportional to the product, $p'_f p'_{o_2}$. This is not an unreasonable approximation, as Hoffmann and Evans (29) have reported a linear increase in chromatographic peak height with O_2 added to the H_2 and column effluent and Sternberg (14) has observed increases in response with O_2 added to the air supply or to the H_2. Multiplication of equation (90) by equation (89) yields

$$I \sim (k_1 f - k_2 f^2)/(2k_3 + (n-1)f) \qquad (91)$$

where

$$k_1 = (0.2\,c - a/2)/(a+b+f) \qquad (92)$$

$$k_2 = (3n+1)/2(a+b+f) \qquad (93)$$

$$k_3 = (a/2 + c) + (b+f) \qquad (94)$$

In the present experiment b + f is the total gas flow through the E.D.F. and is a constant. Therefore, k_1, k_2 and k_3 are constants.

Equation (91) has a maximum which occurs when

$$f = -2k_3/(n-1) + \sqrt{\left(2k_3/(n-1)\right)^2 + 2k_1k_3/\left(k_2(n-1)\right)} \qquad (95)$$

The operating conditions for the experiment were:

$a = 0.5\ cm^3\ sec^{-1}$

$b + f = 0.221\ cm^3\ sec^{-1}$

$c = 6.67\ cm^3\ sec^{-1}$

$n = 4$, for butane

We get therefore -

$$k_1 = 1.50 \text{ (a pure number)}$$
$$k_2 = 9.0 \text{ sec/cm}^3$$
$$k_3 = 7.14 \text{ cm}^3/\text{sec}$$

The maximum detector current should, according to equation (95), occur at $f = 0.0826 \text{ cm}^3/\text{sec}$. The corresponding partial pressure ratio is $p'_f = 11.5\%$ as calculated in equation (90). The observed maximum (see Figure 22) occurred at approximately 30%. This discrepancy is small when one considers that the detector is not an ideal mixing chamber.

Returning to equation (91) we note that

$$2 k_3 = 14.28 \text{ cm}^3/\text{sec}$$

$$(n-1) f \leq 3 \times 0.221 = 0.663$$

Therefore, $(n-1)f/2 k_3 \leq 0.047$ so that equation (91) can be approximated by

$$I \sim G_1 f - G_2 f^2 \qquad (96)$$

where $G_1 = k_1 / 2 k_3$ and $G_2 = k_2 / 2 k_3$

Calibration Data Analysis

The data obtained from the electronic integrator print-out were analyzed by a least squares fit computer program for equation (96), after using equation (90) to convert f to p_f. The curve in Figure 24 is a plot of

$$\Delta q / \Delta t = 30839.1 p_f - 43984.2 p_f^2 \qquad (97)$$

where the detector signal, $\Delta q / \Delta t$, is in integrator counts per 1.137 sec and where the coefficients of p_f and p^2_f are the result of the least squares fit. To convert $\Delta q / \Delta t$ from counts per second to amps the integrator was calibrated against a known current source to obtain a conversion factor of 1977.7×10^9 counts per coulomb. The gram molecular weight of butane is 58 gms. Therefore, the E.D.F. effluent, whose

flow rate is 0.221 cm^3/sec at 1 atm. carries butane into the flame at a mass rate that can be expressed as

$$\dot{m} = 58\ p_f\ (0.221/22.4 \times 10^3) \qquad (98)$$

where the factor in parentheses is the flow rate of butane in moles per second per unit partial pressure (at N.T.P.). We get, therefore,

$$\dot{m} = 5.754 \times 10^{-4}\ p_f \qquad (99)$$

Equation (97) can now be written

$$I = 9.54 \times 10^{-3}\ \dot{m}\ (1-2.47 \times 10^3\ \dot{m}) \qquad (100)$$

which fits the data to within $\pm$ 5%, relative standard deviation. Note that for $\dot{m} << 1/2.47 \times 10^{-3}$ gm sec^{-1} I is directly proportional to $\dot{m}$. The constant of proportionality, 9.54×10^{-3} amp per gm sec^{-1} (i.e. coulombs per gm) is called the "response factor" and is a measure of the ionization efficiency of the flame and is analogous to the constant K in equation (80) of the recombination model. The roll-off parameter, 2.47×10^3 sec/gm is analogous to the coefficient of $\dot{m}$ in the denominator of the right hand side of equation (80). That is, they both determine the value of $\dot{m}$ at which the detector's response deviates from perfect linearity by some prescribed amount (e.g. by 10%). Equation (100) therefore describes the ionization efficiency and the linearity characteristics of the F.I.D. whose basic design features are shown in Figure 9.

Discussion of Calibration Data

It should be emphasized that equation (100) is valid for detection of a continuous stream of butane and for a particular set of H_2, N_2 and air flow rates. In a tabulation of F.I.D. (and thermal conductivity detector) response factors, Dietz (31) has shown that out of 109 hydrocarbons, consisting of normal parafins, branched parafins, cyclopentanes, cyclohexanes, aromatics and unsaturates all but two have the same coulomb per gram response factor to within a few percent. Therefore, if we can assume that the roll-off parameter is also the same for these hydrocarbons, it would appear, at first,

that equation (100) is a valid description of the response characteristics of the F. I. D. in Figure 9. However, the F.I.D. "mixing chamber" analysis implies that the detector's response is not only a function of the instantaneous combustion rate, $\dot{m}$, but depends also on the detector's combustion history. It was shown that the volume enclosed by the detector tower and lid acts as a mixing chamber whose time constant is approximately 2 seconds for the gas flow rates used in the experiment. It can be shown, by applying equation (84) to the F.I.D., that it takes about 2 seconds for the partial pressure of O_2 to recover from the value determined by some fixed hydrocarbon combustion rate to 63% (i.e., $1/e$) of the value determined by H_2 combustion alone. Therefore, the detector "remembers" the hydrocarbon combustion over a period of the order of 2 seconds. This implies that the response curve described in equation (100) and shown in Figure 24 is not the same curve that would be obtained by using discrete injections of butane into the carrier gas, whose complete combustion required less than 2 sec and whose injection frequency was greater than 2 sec. In other words, the characteristics described by the calibration curve will, in general, be determined by the method of calibration as well as the design of the detector.

V. SUMMARY

Gas ionization detectors must include the means for producing and collecting ions and/or free electrons in a flowing gas stream that contains the effluent from a chromatographic separation column. The detector must be designed so that the production or collection (or both) of charged particles is a function of some property of the gases whose detection is desired. The ECD responds in a non-linear way to changes in the gas stream's concentration of molecules whose ability to form stable negative ions reduces the number of free electrons available for collection. The F. I. D. responds in a linear way to the combustion rate of hydrocarbons whose oxidation chemistry includes an ion producing reaction.

The E.C.D. response consists of a loss in standing current. It is desirable, therefore, to maximize the standing current by preventing the back diffusion of atmospheric O_2 through the detector's exhaust port. Oxygen can also cause the E.C.D. to respond to changes in carrier gas flow rate, an undesirable effect which detracts from the detector's usefulness as a concentration detector. Temperature control requirements for the E.C.D. are dictated primarily by the resistance-temperature characteristics of the inter-electrode insulator. At high temperatures, where the Ohm's law current through the glass becomes comparable in magnitude to the standing current, small fluctuations in temperature can cause serious baseline drifting on a chromatogram.

The F. I. D. response consists of an increase in current produced by the chemi-ionization of hydrocarbons in the flame. The overall performance of this detector is determined by the flame's ability to produce ions and the electrode system's ability to compete for ions in the presence of the loss mechanisms, recombination and diffusion.

Both the E.C.D. and the F.I.D. can suffer from "dead volume" effects. The mixing chamber effect in the E.C.D. can cause electron acceptor molecules to reside in the inter-electrode region for a longer period of time than is tolerable for good peak resolution. The mixing chamber effect in the F.I.D. causes the air supply to be diluted with combustion products with a resulting loss in the ionization efficiency of the flame.

VI. CONCLUSIONS

The ultimate test of merit for a gas chromatographic detector is its performance in a G.C. system. Calibration methods and response characteristics tests must, therefore, be designed with chromatographic requirements in mind. A distinction can be made between static and dynamic response characteristics. The former is

concerned with the questions, what is the response of an E.C.D. to a fixed (in time) concentration of sample and what is the response of the F.I.D. to a constant hydrocarbon combustion rate? Dynamic characteristics, on the other hand, are determined by a detector's ability to respond to rapid changes in concentration or mass rate. Response factors can be used for specifying static characteristics. Dynamic characteristics can be specified by detector time constants.

The problems of measuring or calculating response factors are many. In the case of the E.C.D. response factors were not investigated in this thesis. However, it is possible that for electron attachment reactions that are shifted strongly to the right (See Equation (3)) the Beer's law interpretation may be valid, while for ions with smaller electron affinities the Wentworth-Becker equilibrium theory may be more appropriate. In view of the E.C.D.'s sensitivity to O_2 and to carrier gas density, measurements of electron capture coefficients or response factors should be made under conditions of constant pressure and with O_2 back diffusion eliminated. Furthermore E.C.D. response factors can only be meaningful if the pressure and temperature of the detector are specified. Three body electron attachment reactions, as described by Pack and Phelps (32), are especially pressure sensitive and electron attachment reactions in general can be expected to depend on temperature.

Flame ionization detector response factors can only be meaningful when the H_2, air and carrier gas flow rates are specified relative to a particular detector design. A change in burner jet diameter will produce, among other things, a change in flame gas velocity which, as we saw in the diffusion flame studies, will produce a change in flame height. A change in flame height means a re-positioning of the ion production sites relative to the collector electrode and, in view of the ion loss by recombination studies, an effect on the response characteristics of the detector can be anticipated. Therefore, a set of optimum gas flow parameters for one jet diameter will not, in general, be optimum for another.

The measurement of F.I.D. response factors by the combustion of a continuous

stream of hydrocarbon vapor from an E.D.F. will yield meaningful but not necessarily useful results. The combustion of a particular hydrocarbon at a given rate for one second will not, in general, yield the same coulombs per gram response factor as the combustion of the same hydrocarbon at the same rate for an interval of one minute. That is, calibration data generated by using the E.D.F. method may be influenced by a degree of O_2 depletion that does not exist when discrete syringe injections are detected. Furthermore, calibration data that is specified in terms of a "total charge collected versus total weight injected" response curve may be of limited use for correlating instantaneous response to instantaneous combustion rate.

Several examples of detector time constants were cited in this thesis. In the case of the E.C.D. the detector can be viewed as a mixing chamber. The relation between detector time constant and peak broadening (i.e., loss of resolution) has been analyzed by Sternberg (11). The hot collector electrode experiment provides another example of peak broadening due to a large time constant. While thermocouple detectors do not fall in the category, "Ionization Detectors", the discussion of thermal effects did suggest the use of flame temperature as a means of G.C. detection. Primavesi (33) has, in fact, reported on the use of a thermocouple detector. A computed relation between the temperatures of a hypothetical flame and a spherical mass of platinum was seen in Figure 13. Equations (53), (54) and (55) show that as the time constant 1/B is made smaller, by reducing the mass of platinum, the temperature of the sphere or a thermocouple with equivalent heat capacity can be made to follow the flame temperature more faithfully.

The question of optimum electrode spacing does not have a simple answer. The best electrode configuration for a given burner design and set of gas flow rates must be found empirically. We have seen some of the problems that can arise when the F.I.D. collector is too close to or too far from the flame. Simple systems, such as the laminar flow air pipe detector, enable one to analyze response data in terms of conceptually isolatable mechanisms. In the final analysis, however, more complicated configurations may be necessary for achieving a desired set of detector characteristics.

VII. REFERENCES

1. J. E. Lovelock and S. R. Lipsky, J. Am. Chem. Soc. 82, 431 (1960)

2. "Nuclear Engineering Handbook", 1st ed., H. Etherington, Ed. (McGraw-Hill, New York, 1958) pp 7-5 and 7-33.

3. A. von Engle, "Ionized Gases" (Clarendon Press, Oxford, 1965)

4. J. E. Lovelock, Anal. Chem. 35, 474 (1963)

5. J. D. Cobine, "Gaseous Conductors" (Dover Publications, Inc., New York, 1958)

6. J. E. Lovelock, Anal. Chem. 33, 162 (1961)

7. R. H. Healy and J. W. Reed, "The Behaviour of Slow Electrons in Gases" (Amalgamated Wireless, Ltd., Sydney, 1941)

8. W. E. Wentworth and R. S. Becker, J. Am. Chem. Soc. 84, 4263 (1962)

9. M. Scolnick, J. Chromatog. Sci. 7, 300 (1969)

10. G. O. Jones, "Glass" (Methuen & Co. Ltd., London, 1956)

11. J. C. Sternberg in "Advances in Chromatography", J. C. Giddings and R. Keller, Eds. (Marcel Dekker, New York, 1966) Vol. 2

12. H. F. Calcote in "Ninth Symposium (International) on Combustion" (Academic Press, New York, 1963)

13. J. A. Green and T. M. Sugden, ibid.

14. J. C. Sternberg, W. S. Gallaway and D. T. L. Jones in "Gas Chromatography, 3rd International Symposium", N. Brenner, Joseph E. Callen and Marvin D. Weiss, Eds. (Academic Press, New York, 1962)

15. S. P. Burke and T. E. W. Schumann, Ind. Eng. Chem. 20, 998 (1928)

16. J. A. Fay, J. Aero. Sci. 21, 681 (1954)

17. A. G. Gaydon and H. G. Wolfhard, "Flames: Their Structure, Radiation and Temperature" (Chapman and Hall, London, 1953)

18. "Chemical Engineer's Handbook", 4th ed., J.H. Perry, Ed (McGraw-Hill, New York, 1954) p. 14-22

19. W. H. McAdams, "Heat Transmission" (McGraw-Hill, New York, 1954)

20. "Handbook of Chemistry and Physics", 43rd ed., C. D. Hodgman, Ed., (Chemical Rubber Co., Cleveland, Ohio, 1962).

21. F. M. Page, Trans. Faraday Soc. 56, 1742 (1960)

22. I. G. McWilliams, J. Chromatog. 6, 110 (1961)

23. L. Ongkiehong in "Gas Chromatography 1960", R. P. W. Scott, Ed., (Butterworths, London, 1960)

24. D. H. Desty, C. J. Geach and A. Goldup, ibid.

25. R. A. Dewar, J. Chromatog. 6, 312 (1961)

26. R. Kaiser, "Gas Phase Chromatography", Vol. 2 (Butterworths, Washington, 1963)

27. E. Cohen, E. Parzen, and D. Bailey, J. Gas Chromatog. 1, (8), 14 (1963)

28. J. E. Lovelock, in "Gas Chromatography 1960", R. P. W. Scott, Ed. (Butterworths, Washington, 1960)

29. R. L. Hoffman and C. D. Evans, J. Gas Chromatog. 4, (8), 318 (1966)

30. M. Scolnick, "The Radioactive Foil Electron Capture Detector" (Tech. Bulletin 132-67, Varian Aerograph, Walnut Creek, California, 1967)

31. W. A. Dietz, J. Gas Chromatog. 5 (2), 68 (1967)

32. J. L. Pack and A. V. Phelps, J. Chem. Phys. 44 1870, (1966)

33. G. R. Primavesi, G. F. Oldham and R. J. Thompson in "Gas Chromatography 1958", D. H. Desty, Ed.(Butterworths, London, 1958)

34. E. Jahnke and F. Emde, "Tables of Functions" (Dover Publications, New York, 1958)

35. F. Reif, "Fundamentals of Statistical and Thermal Physics" (McGraw-Hill, New York, 1965)

LIST OF FIGURES

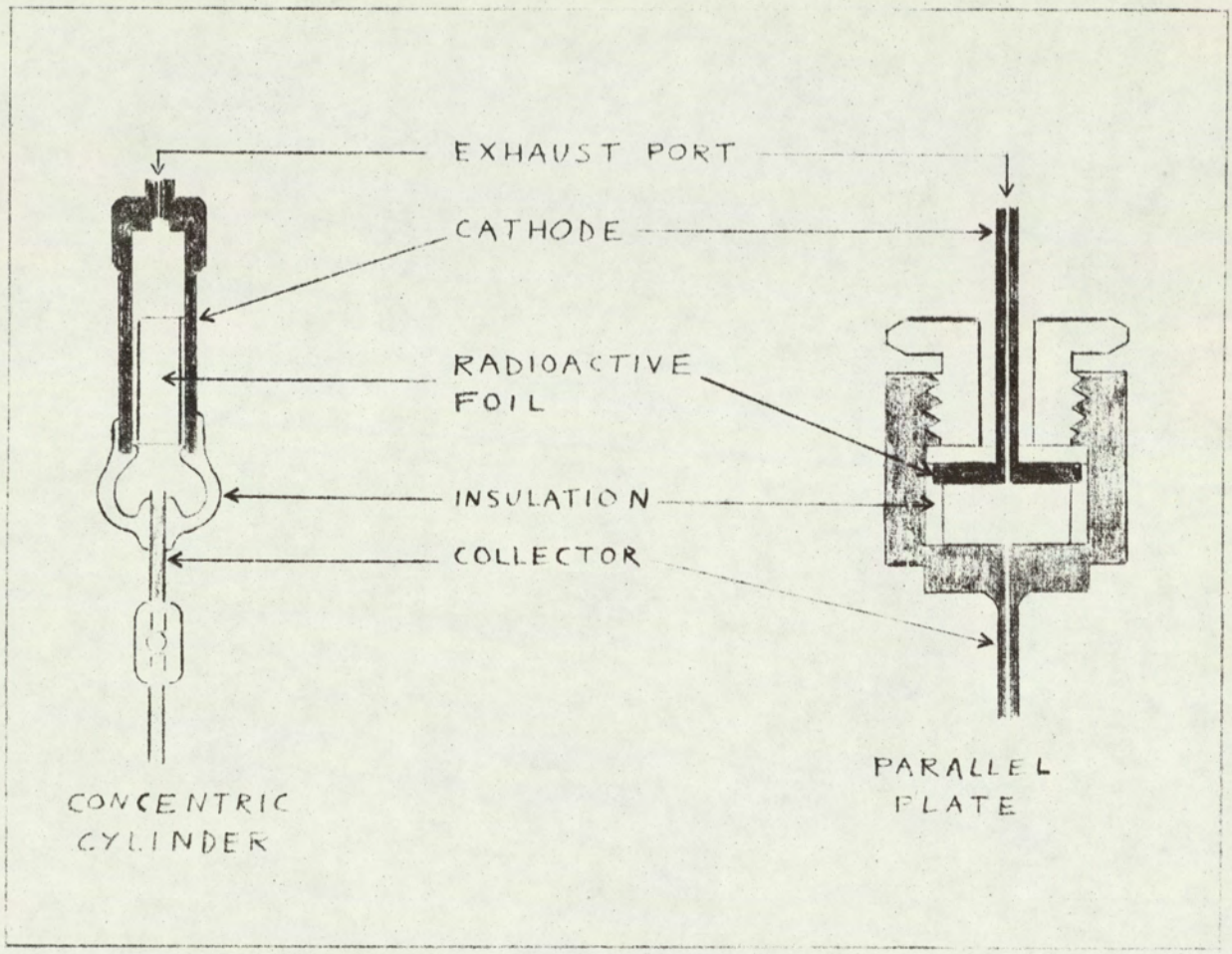

Figure 1. Two electron capture detector design geometries

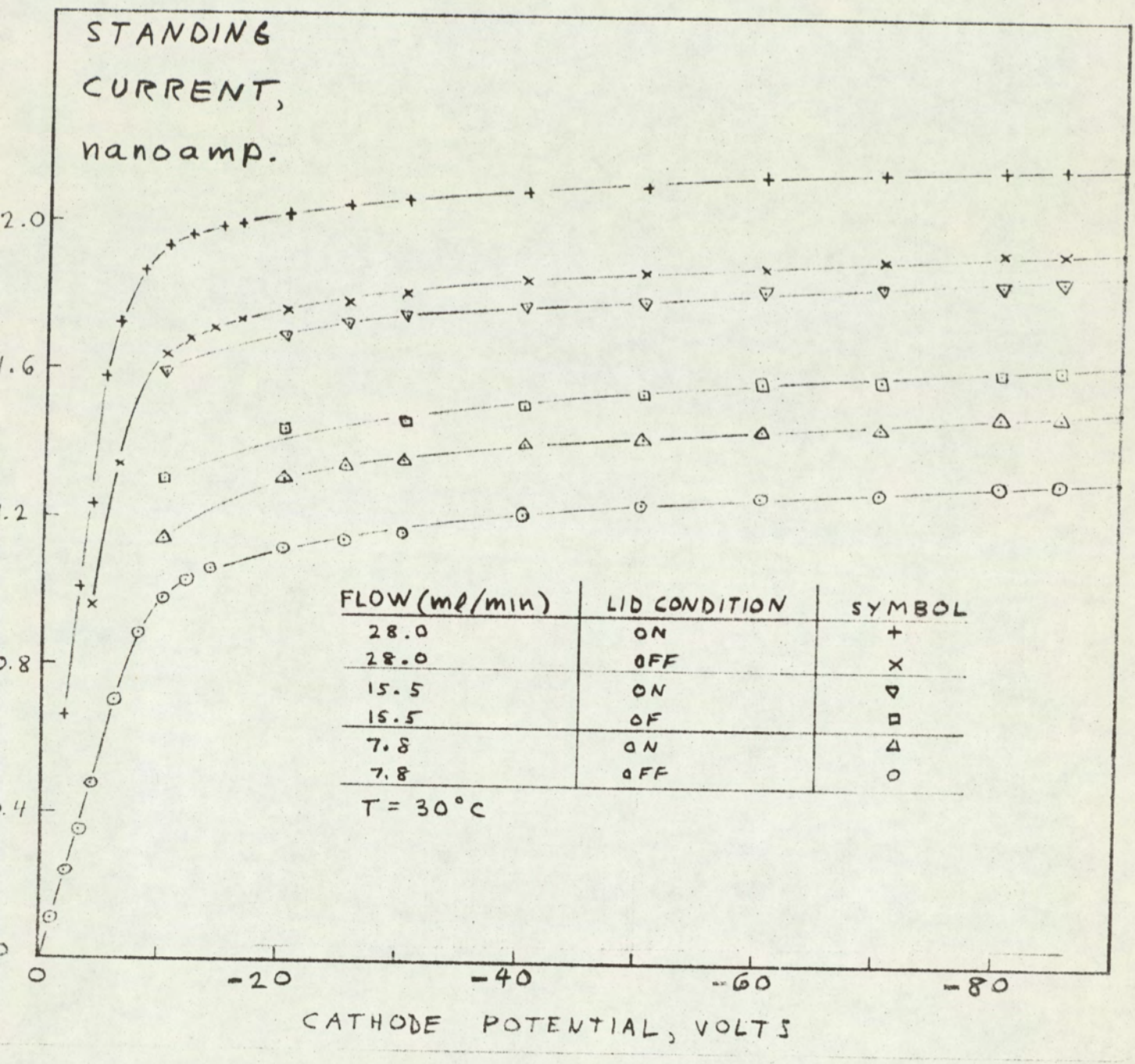

Figure 2. The effects of O_2 back diffusion on the standing current of a Ni^{63} concentric cylinder E.C.D. Exhaust port dimensions: ID = 0.045", length = 0.15".

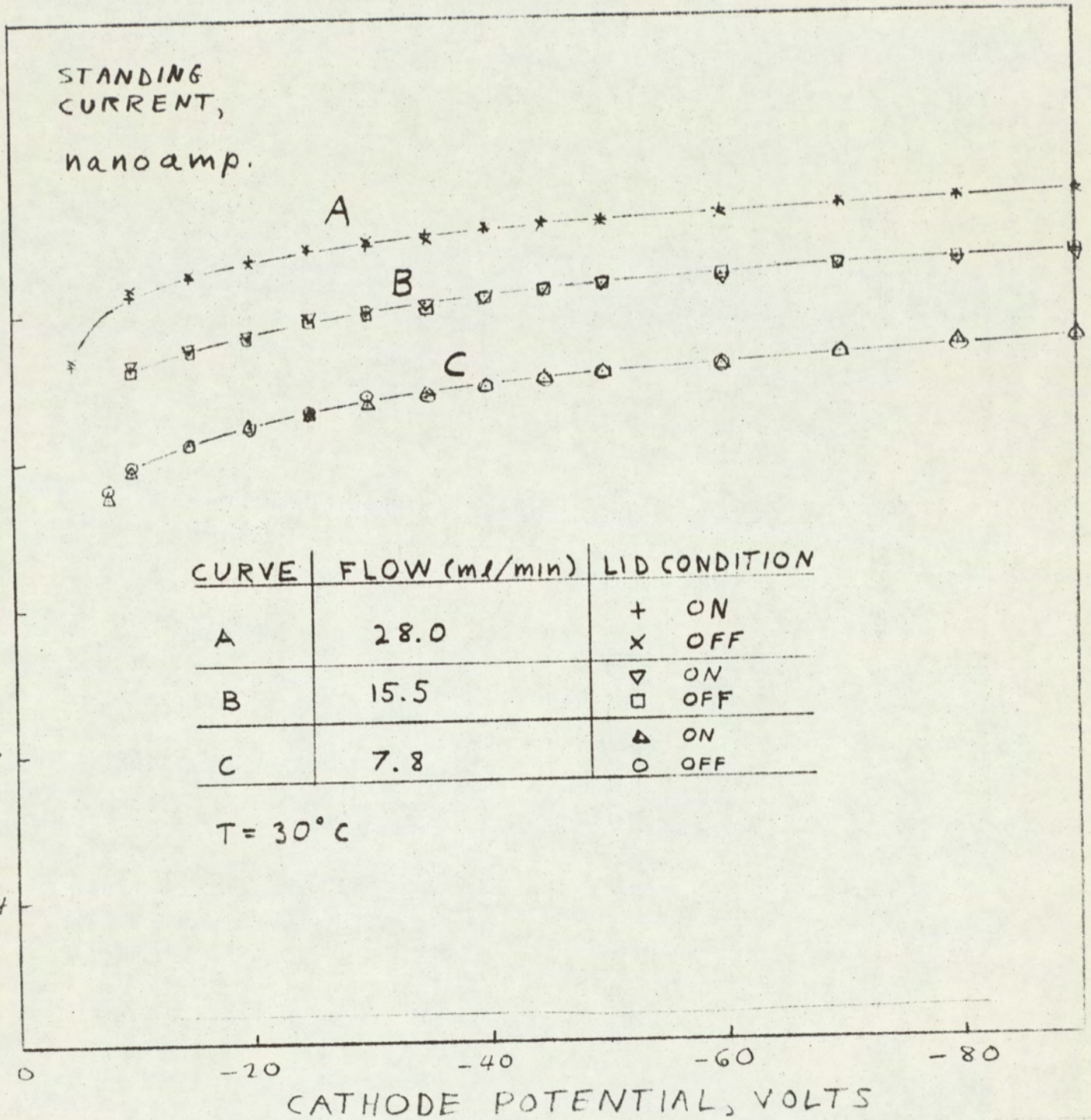

Figure 3. Standing current curves with smaller exhaust port, showing reduction in effects of O_2 back diffusion. Exhaust port diameter = 0.01".

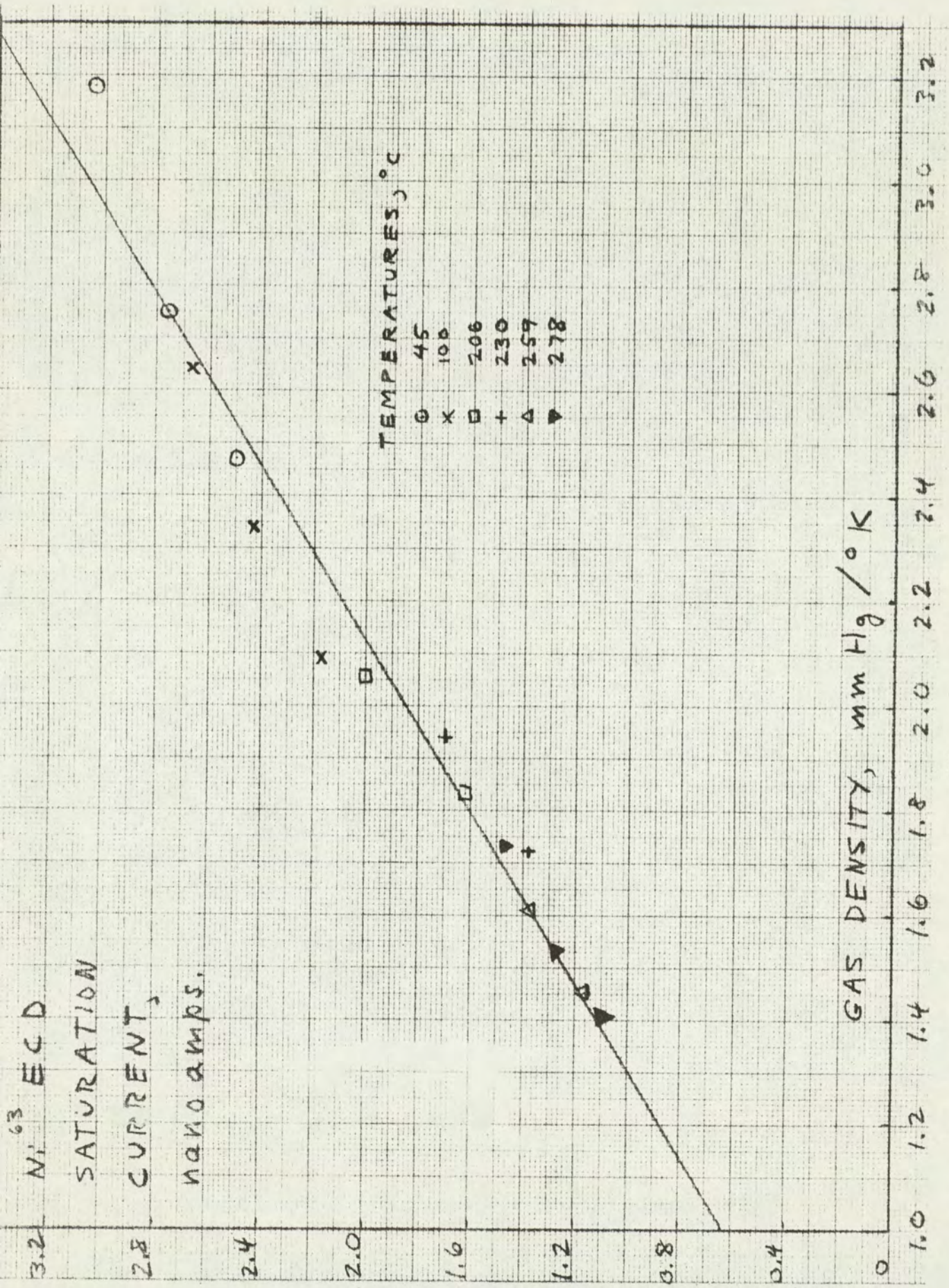

Figure 4. Saturation standing current for Ni^{63} concentric cylinder E.C.D. as a function of carrier gas density, absolute pressure/absolute temperature.

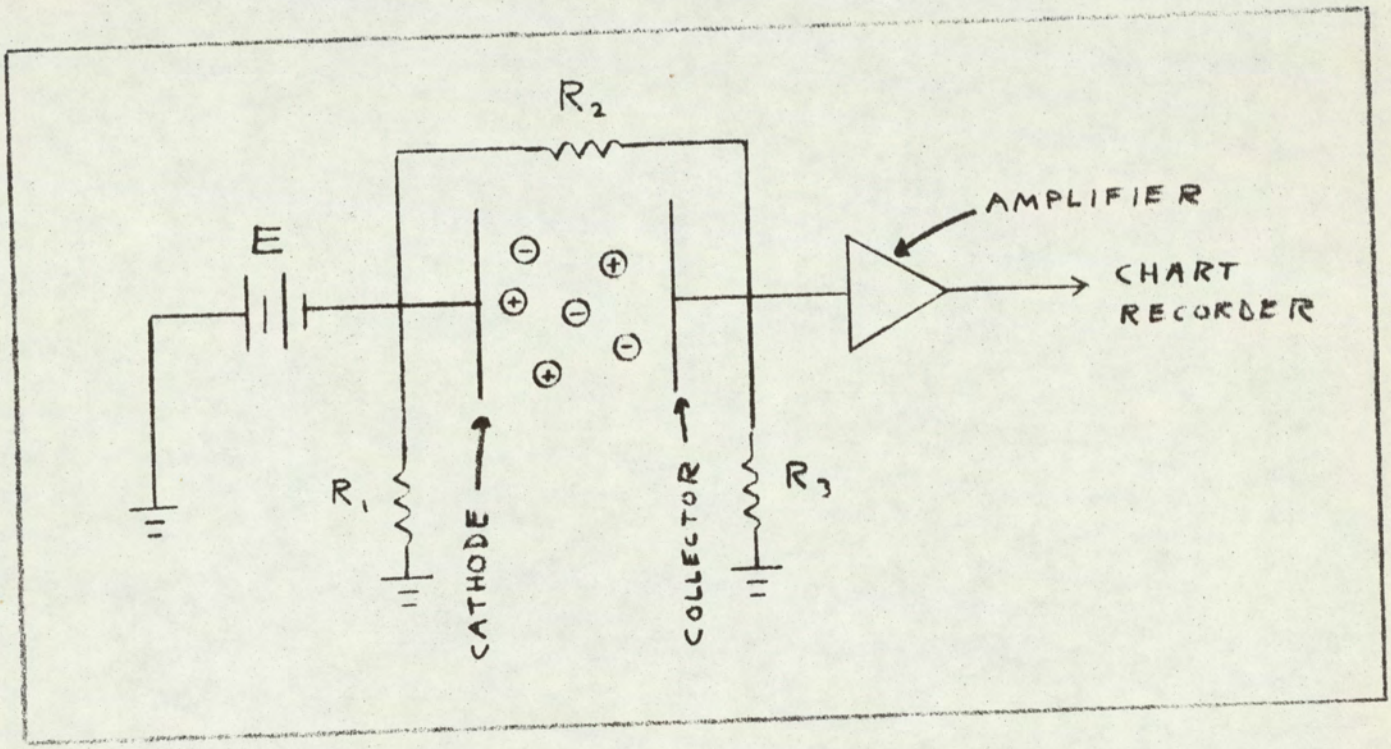

Figure 5. Schematic representation of E.C.D. equivalent circuit.

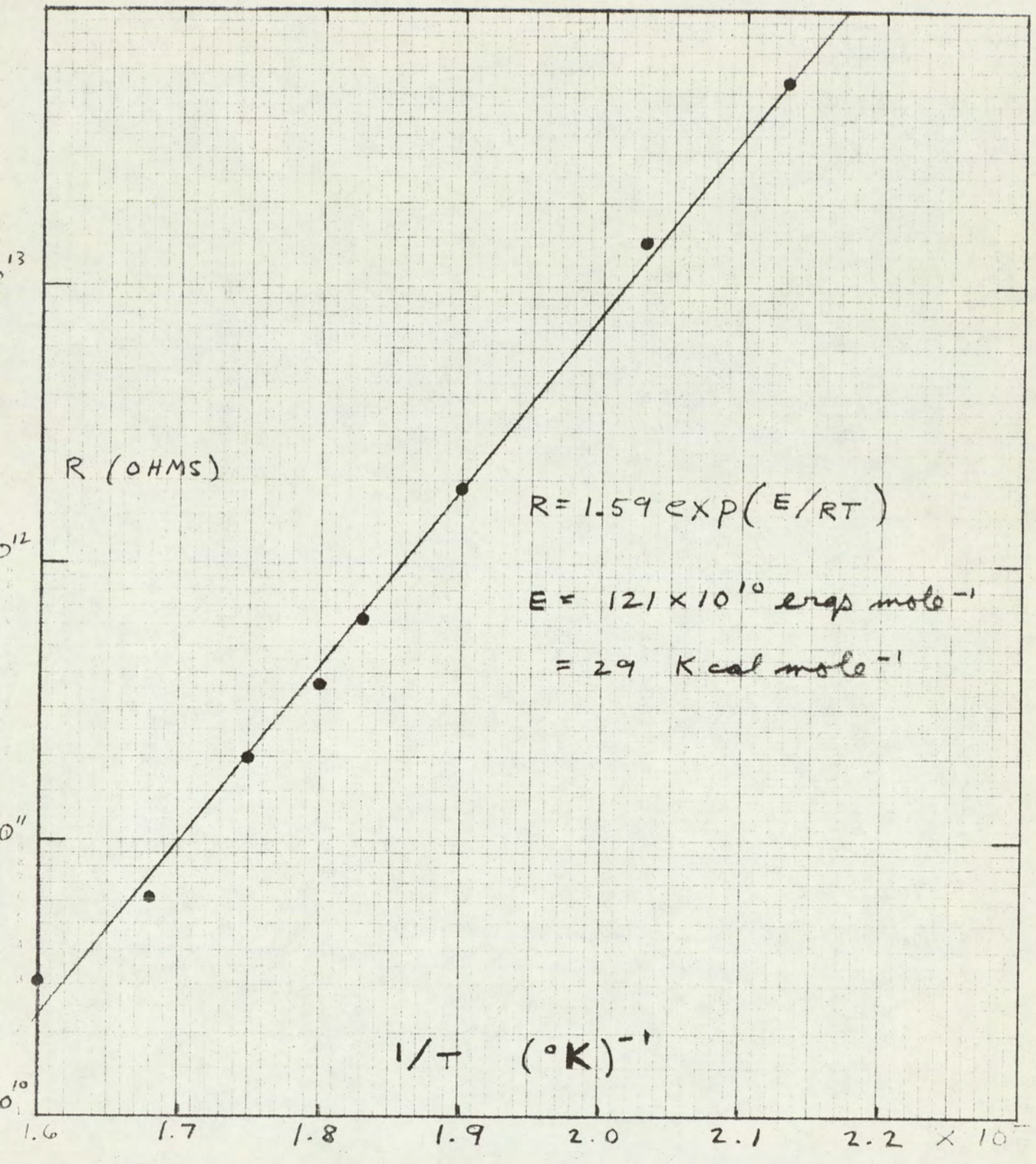

Figure 6. Electrical resistance of interelectrode glass insulator as a function of reciprocal temperature.

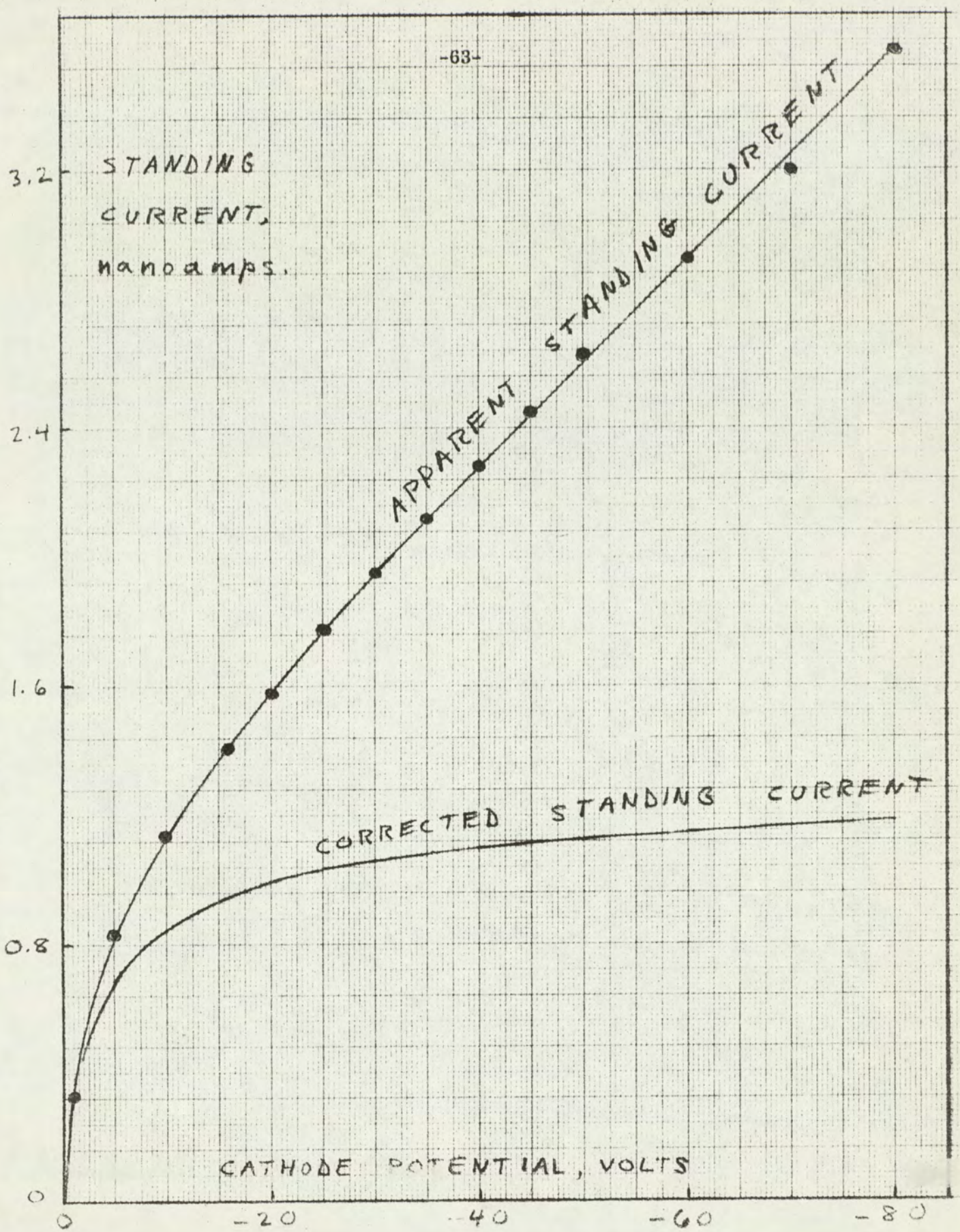

Figure 7. The apparent standing current of a Ni^{63} E. C. D. at 342°C and the real standing current, corrected for the finite conductivity of the inter-electrode glass insulator.

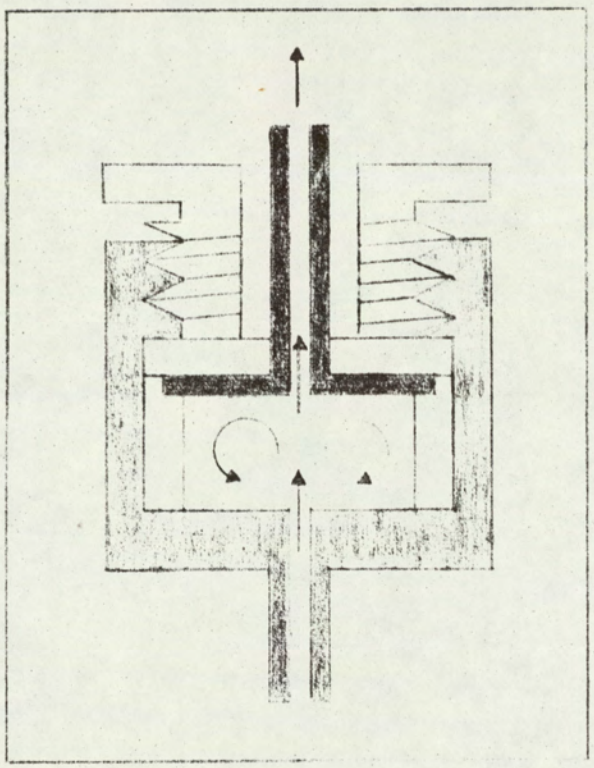

Figure 8. Mixing chamber effect in a parallel plate E.C.D.

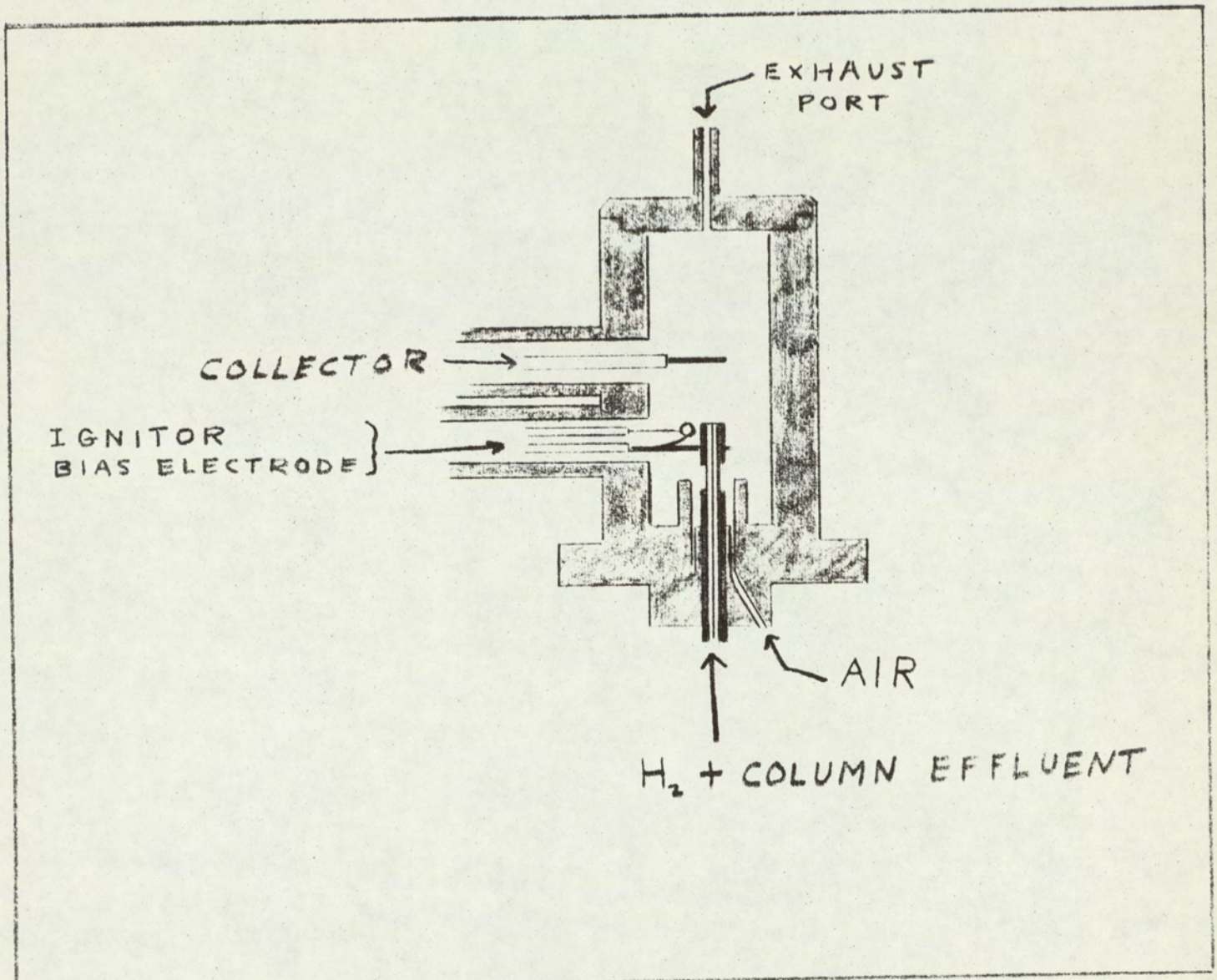

Figure 9. Basic flame ionization detector design features.

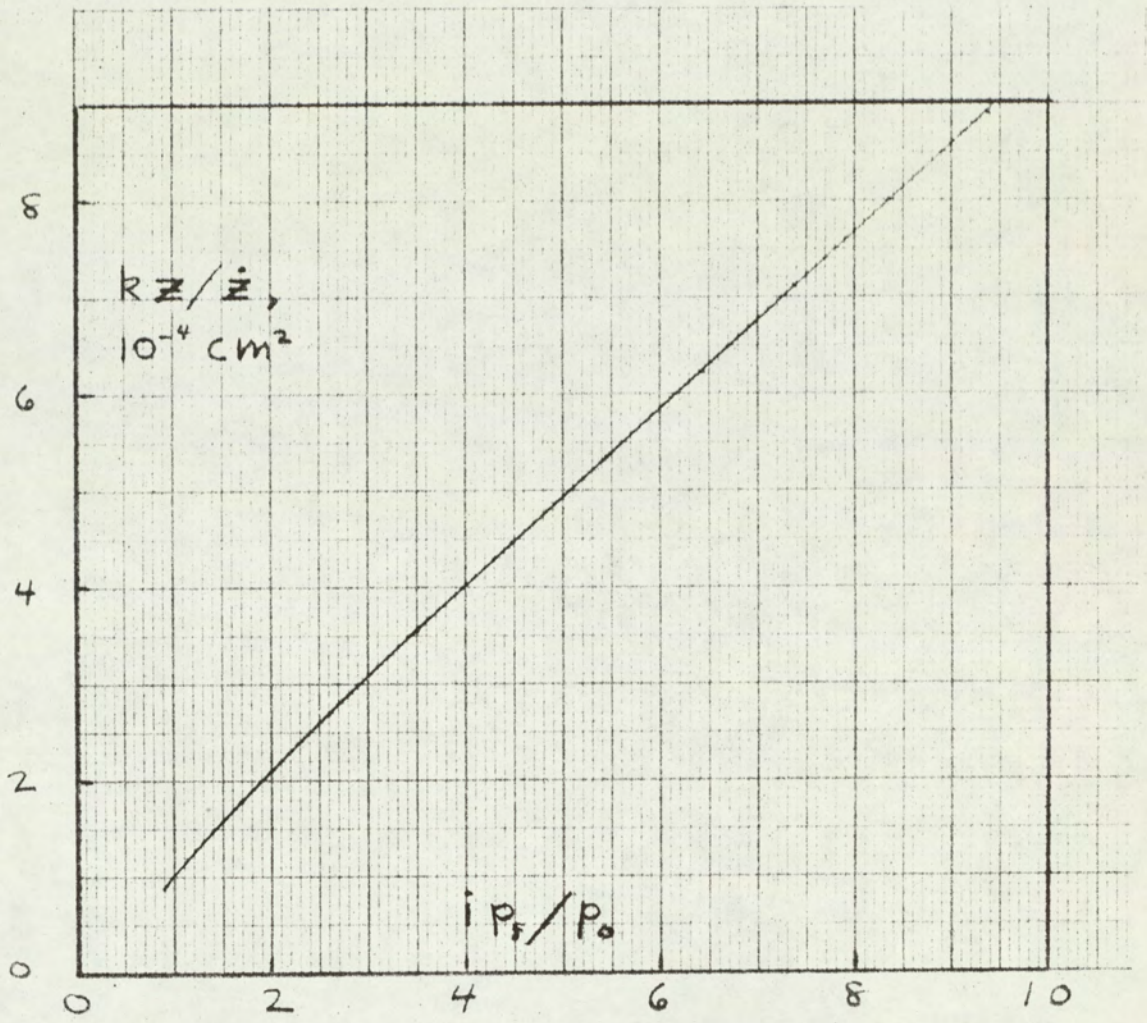

Figure 10. Computed relationship for diffusion flame k = coefficient of interdiffusion, z is the height of the flame, and $\dot{z}$ is the linear gas velocity. p_f is the partial pressure of fuel in the unburnt jet gases and p_o is the partial pressure of O_2 in the air supply. i is the molar ratio of O_2 to fuel for stoichiometric combustion.

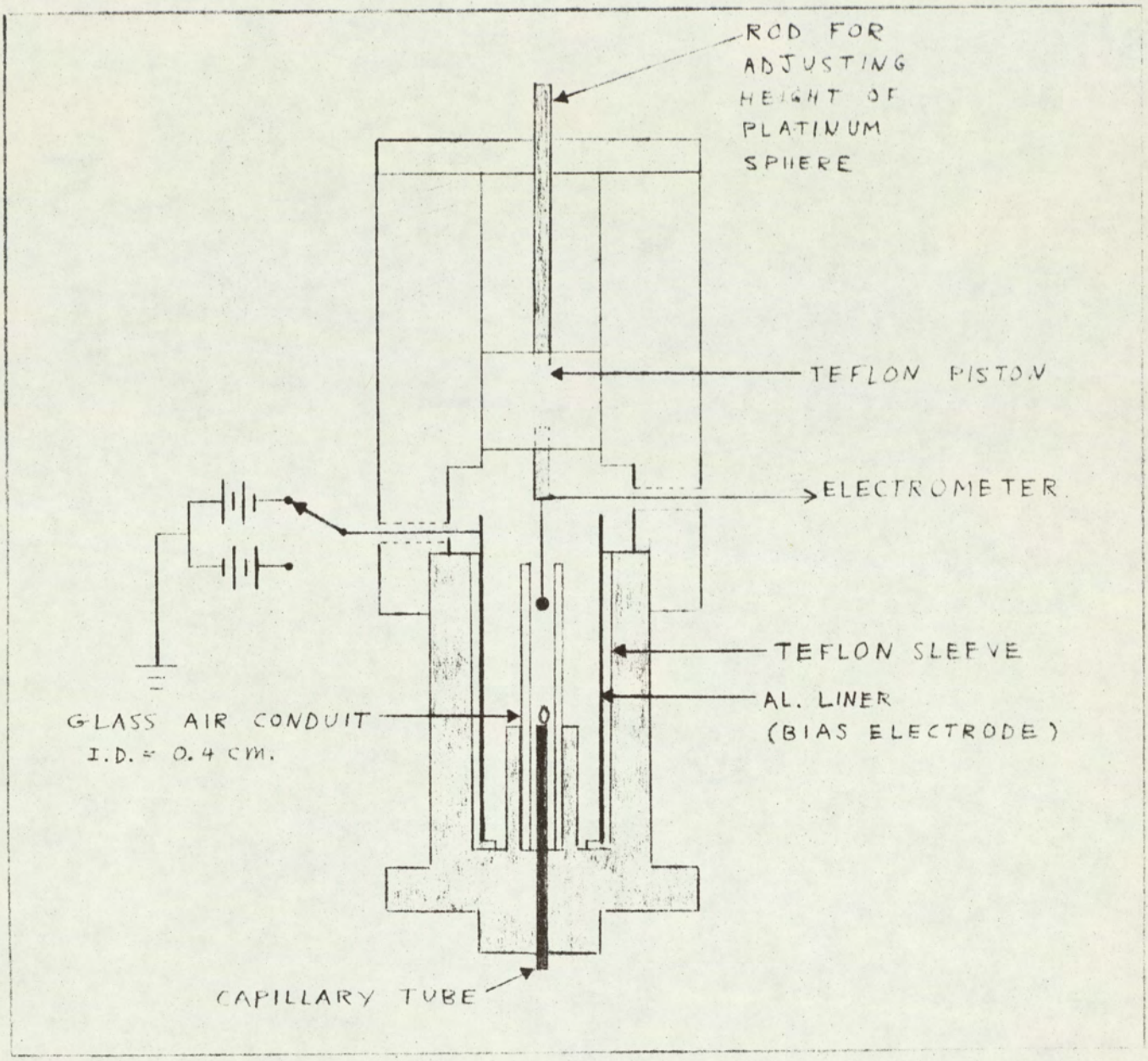

Figure 11. Detector design for hot collector experiment. Air is supplied to the annular region between the capillary tube and glass conduit through ducts (not shown) in the detector base.

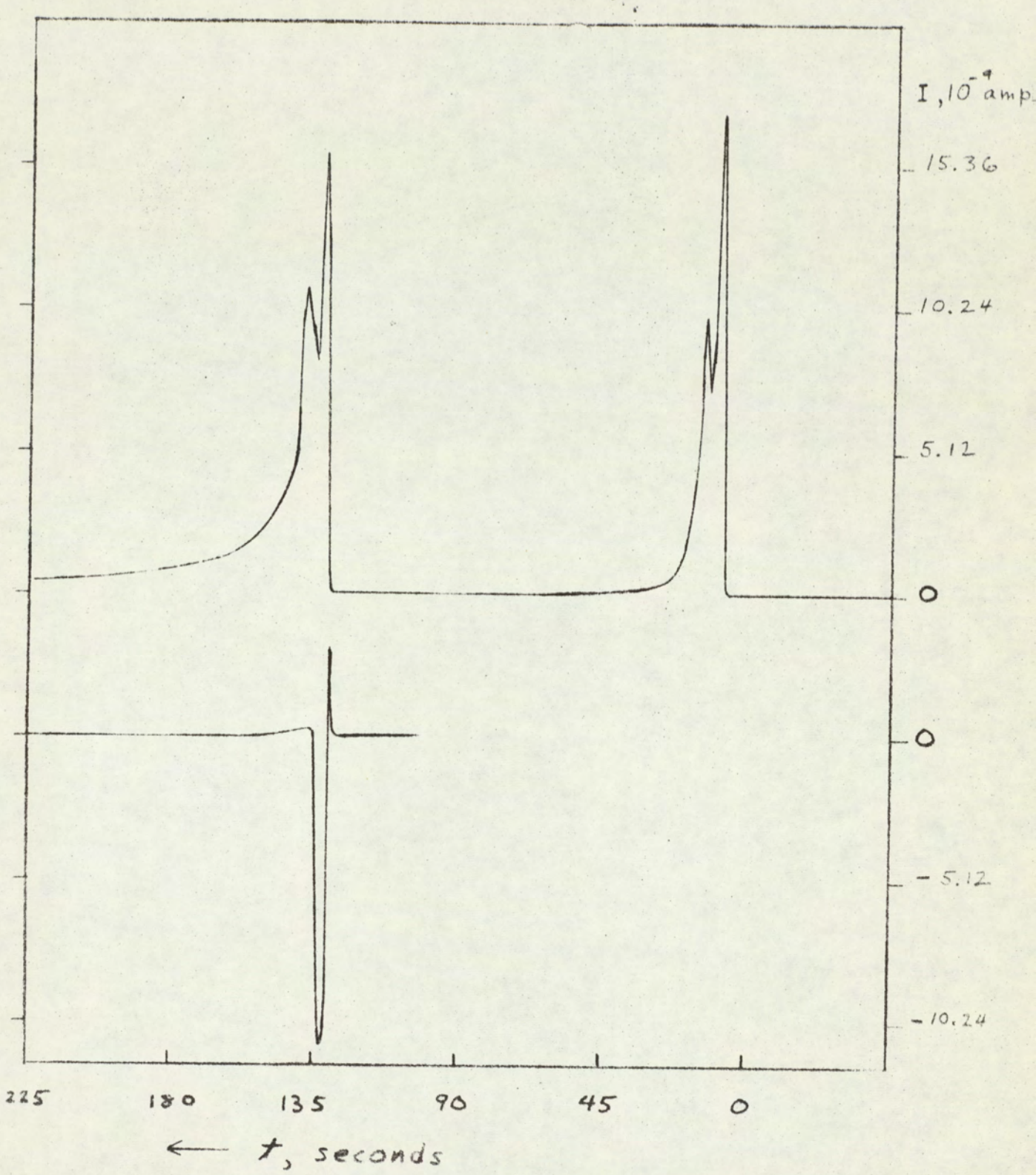

Figure 12. Benzene peaks obtained with heated collector electrode. Upper peaks were obtained with the aluminum foil biased positively (with respect to collector). Lower peak was obtained with a negatively biased foil.

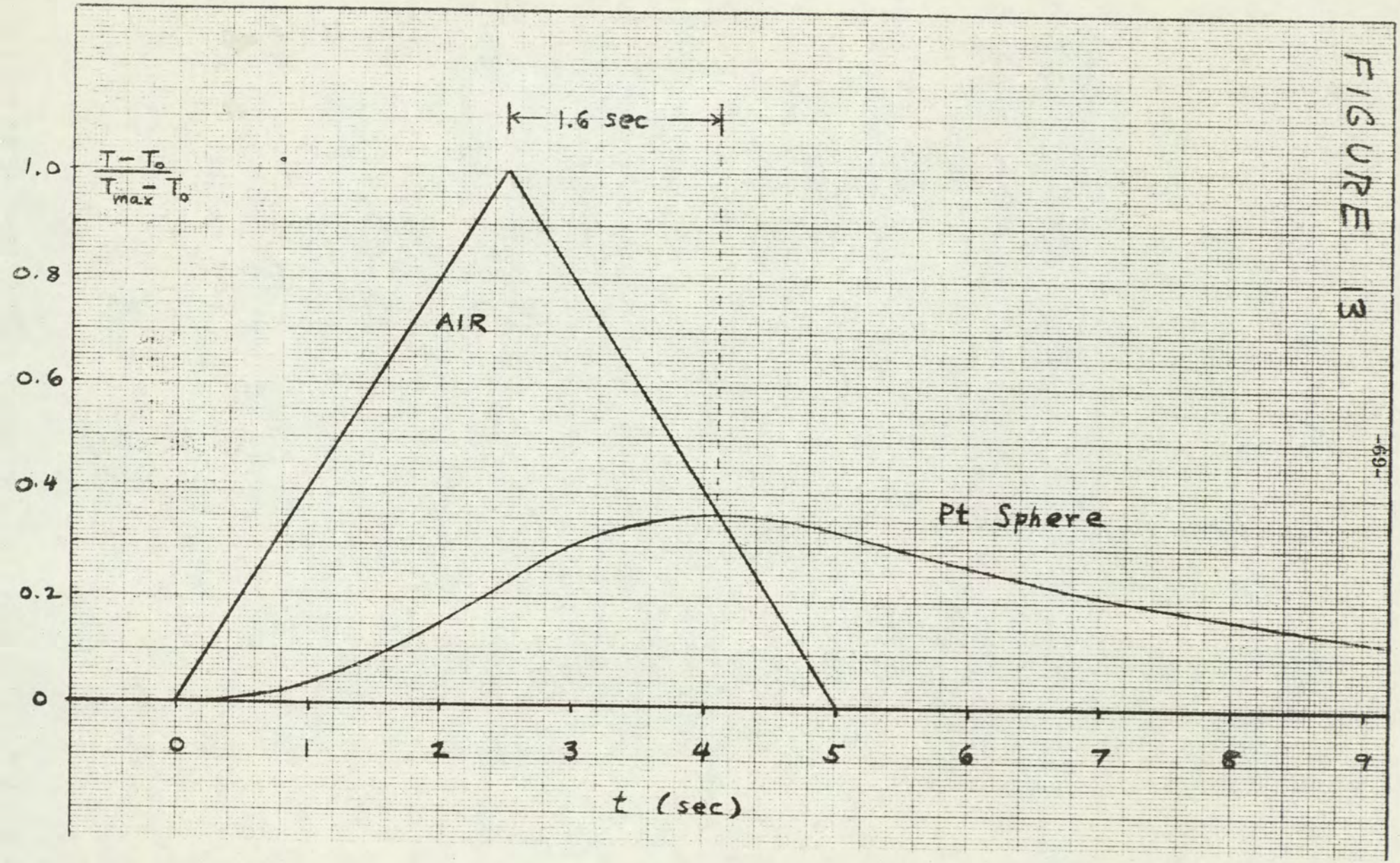

Figure 13. Computed Pt. sphere temperature as a function of a hypothetical air temperature function.

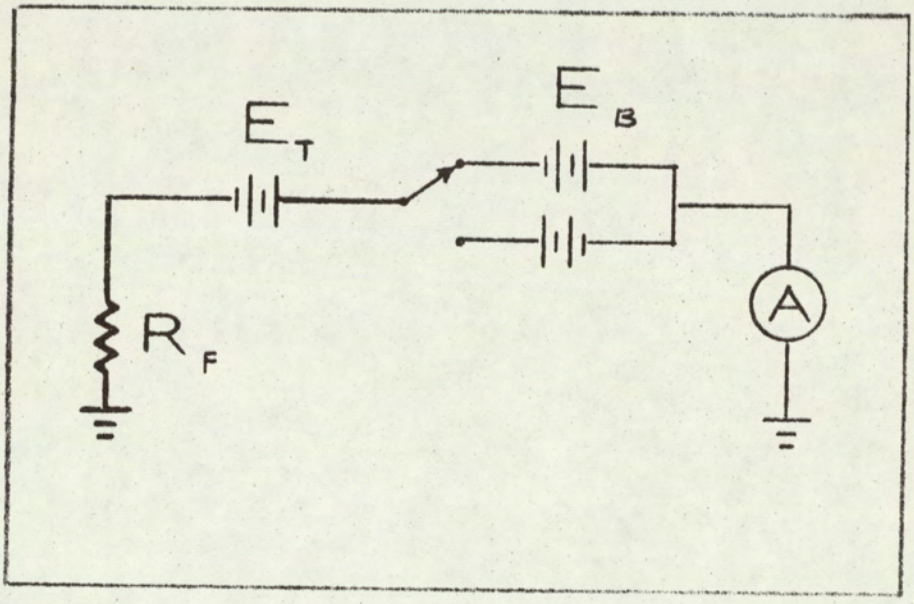

Figure 14. Equivalent circuit for detector shown in Figure 11. E_T represents E.M.F. developed by "thermocouple". E_B represents the effect of biasing the aluminum foil. R_F is the effective resistance of the gases between the burner jet and the collector electrode.

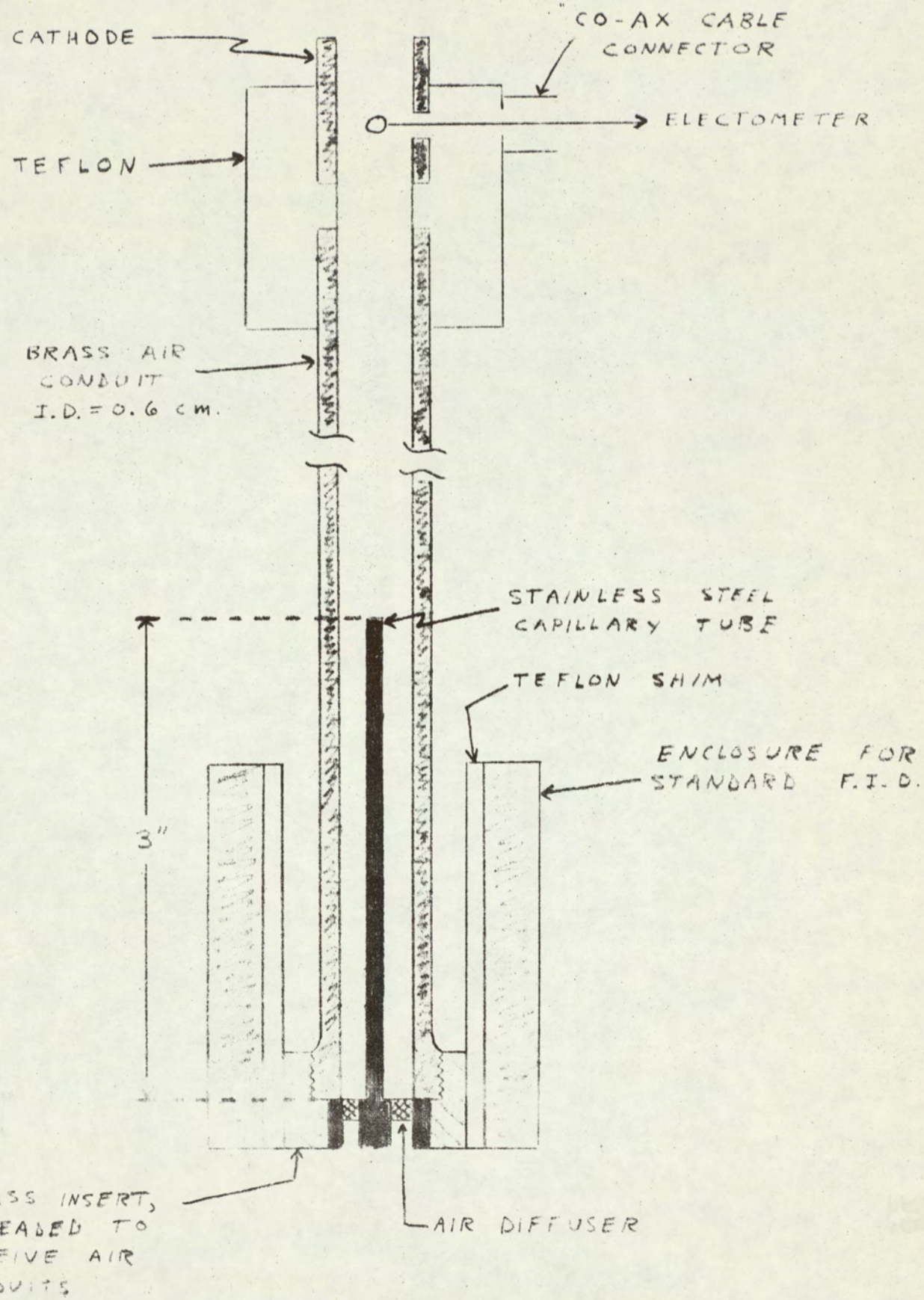

Figure 15. Detector design for ion recombination and diffusion studies.

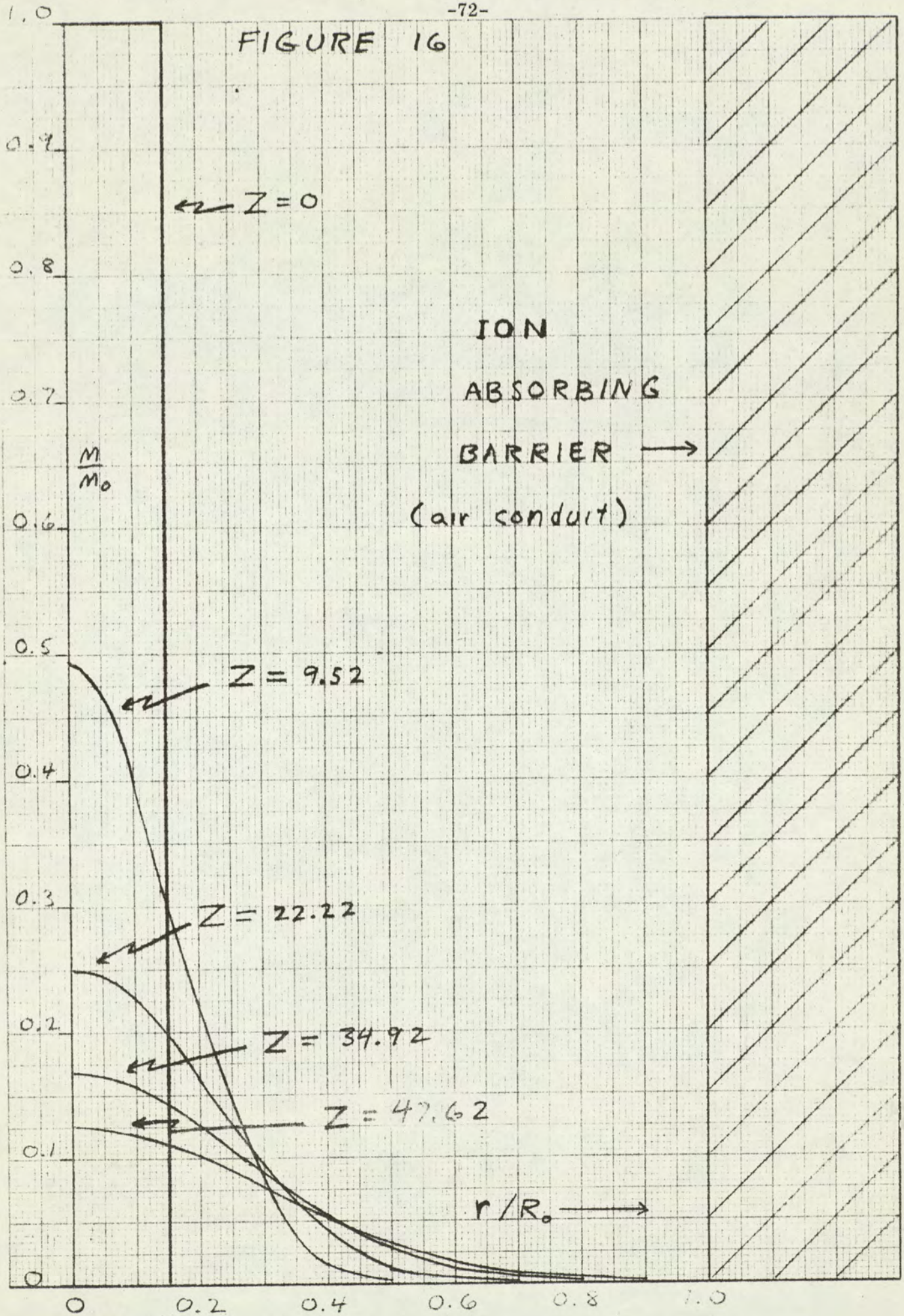

Figure 16. Computed relative ion density distributions.

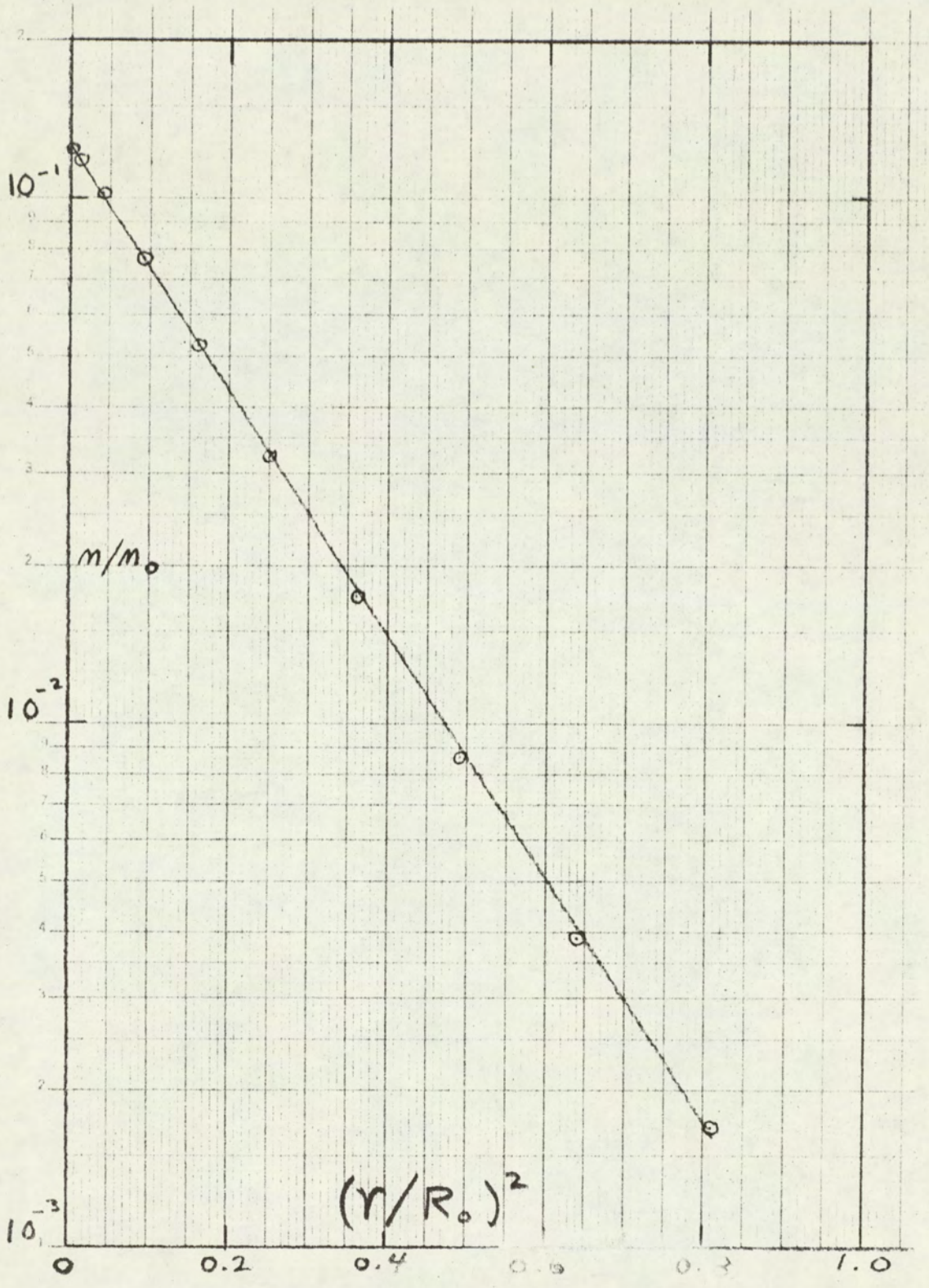

Figure 17. Computed relative ion density distribution at z = 47.62 cm.

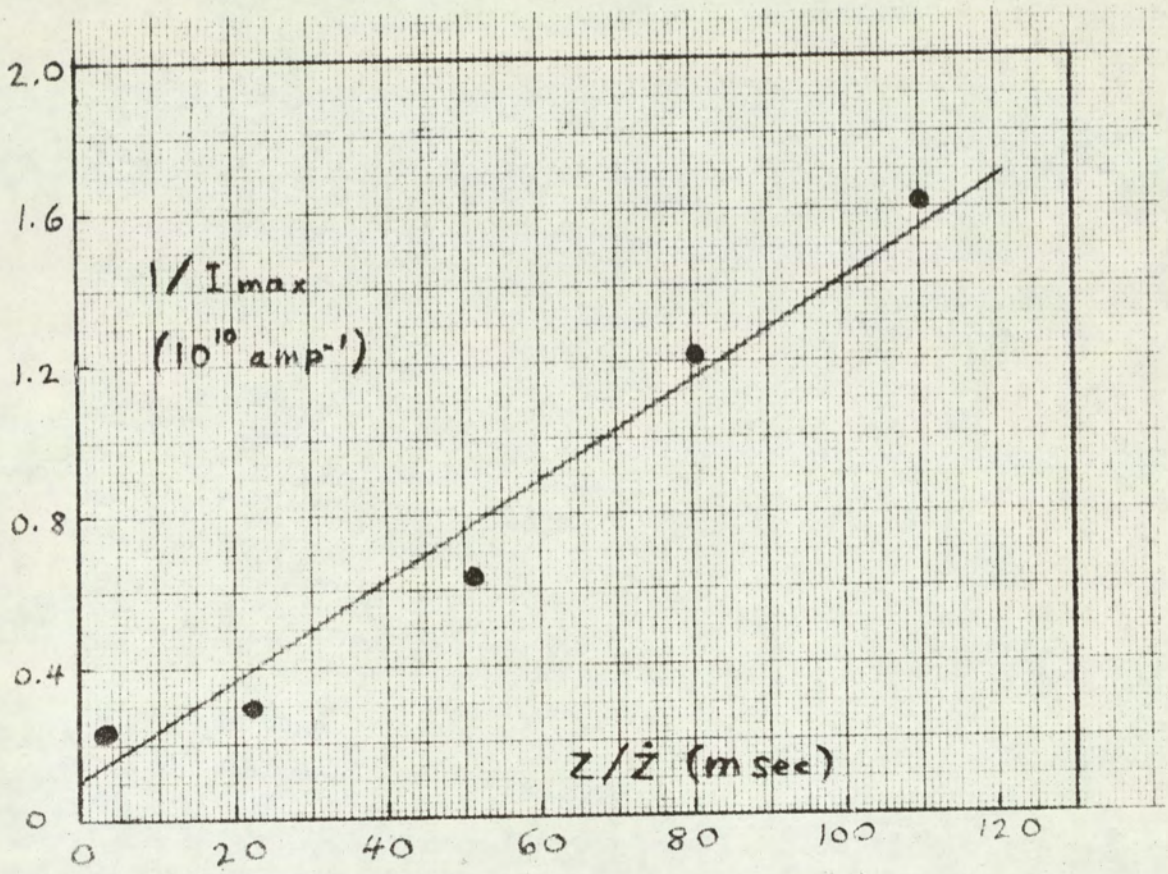

Figure 18. Reciprocal hexadecane peak height versus time required for ions to travel from flame to collector electrode.

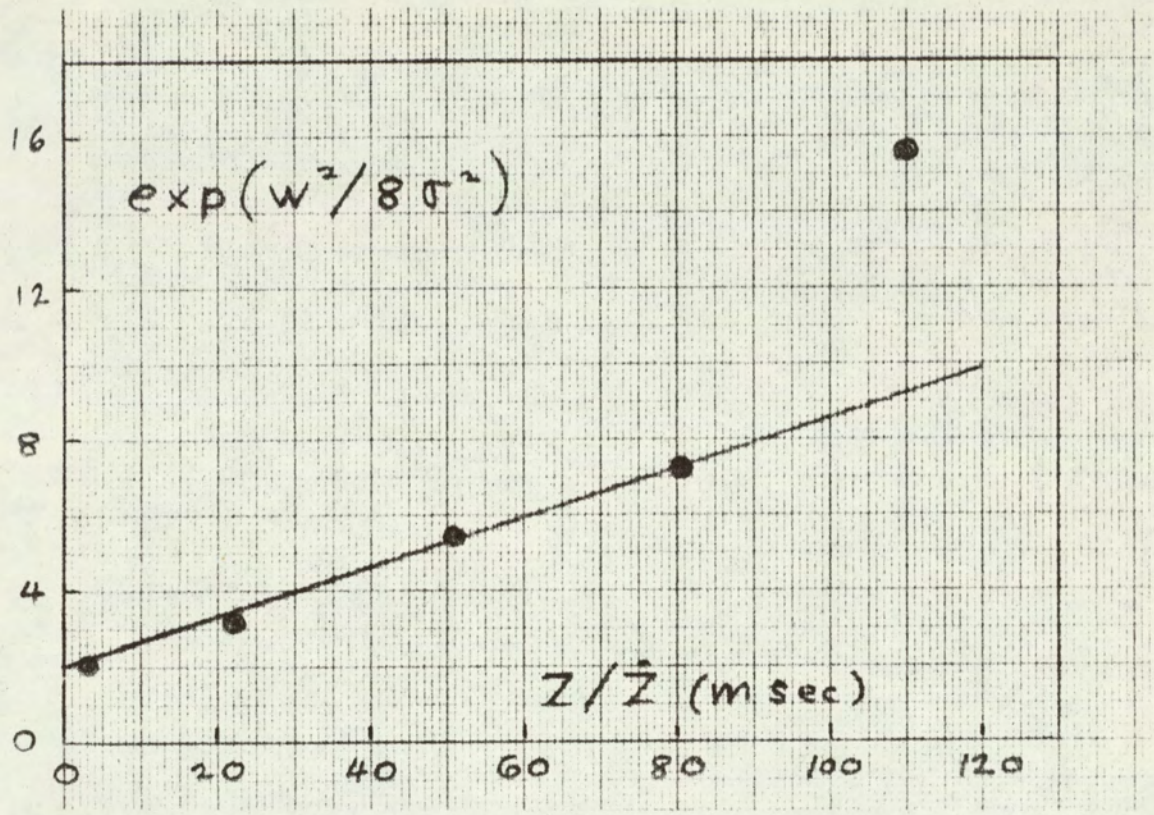

Figure 19. Chromatographic peak width data, showing good agreement with recombination theory. W is hexadecane peak width at half height.

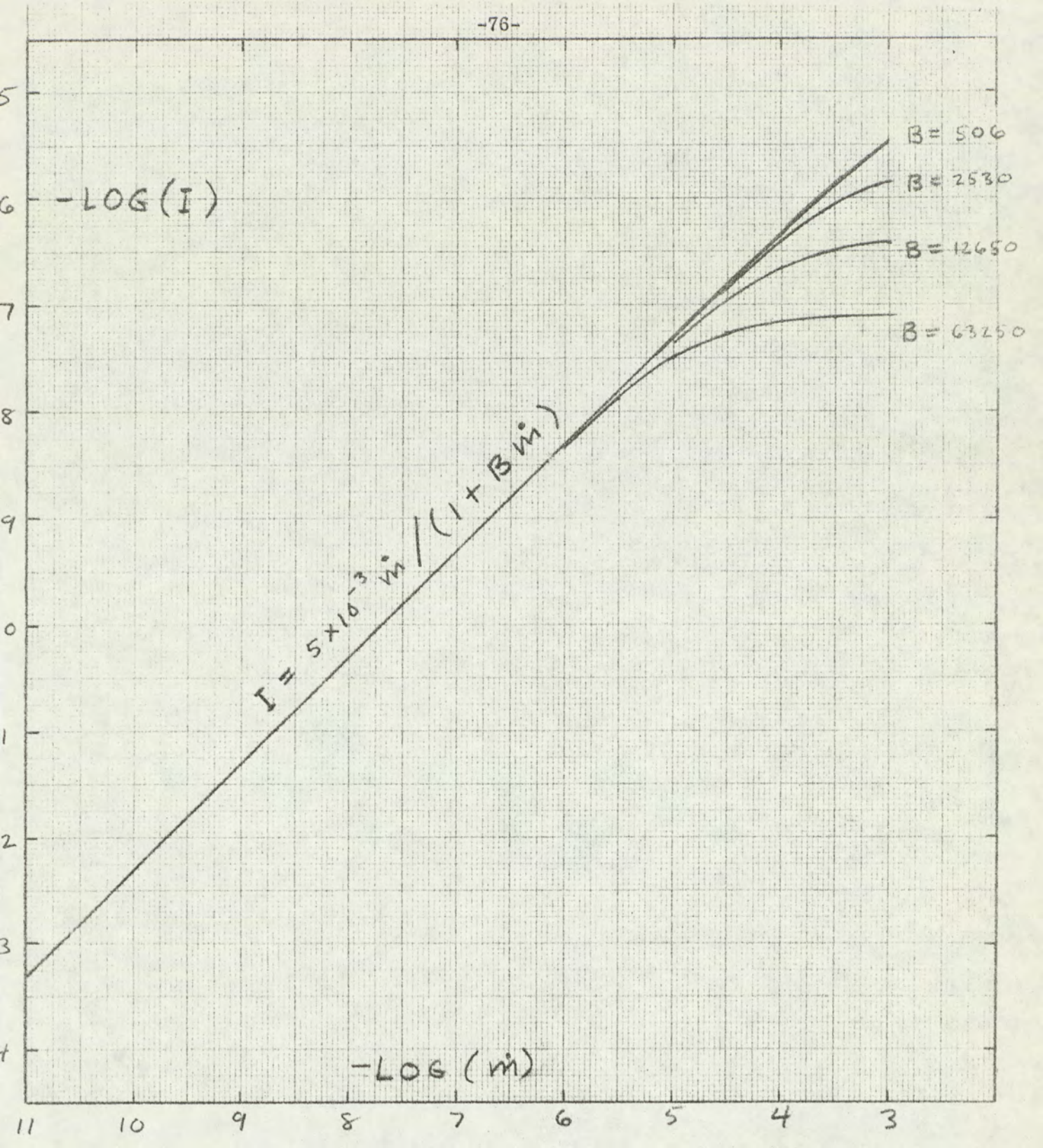

Figure 20. Hypothetical F.I.D. response curve derived from recombination theory.

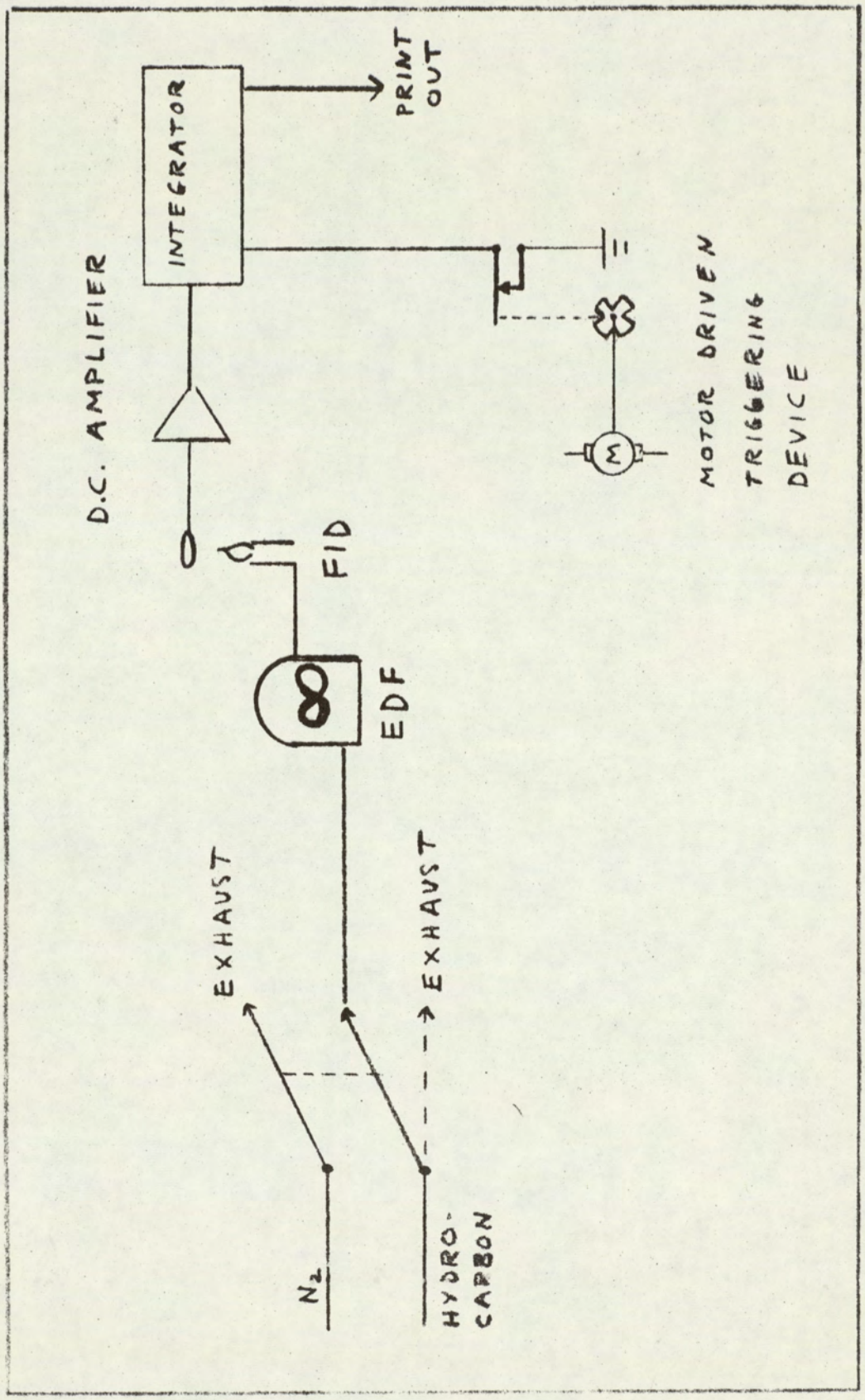

Figure 21. Schematic of F.I.D. calibration system.

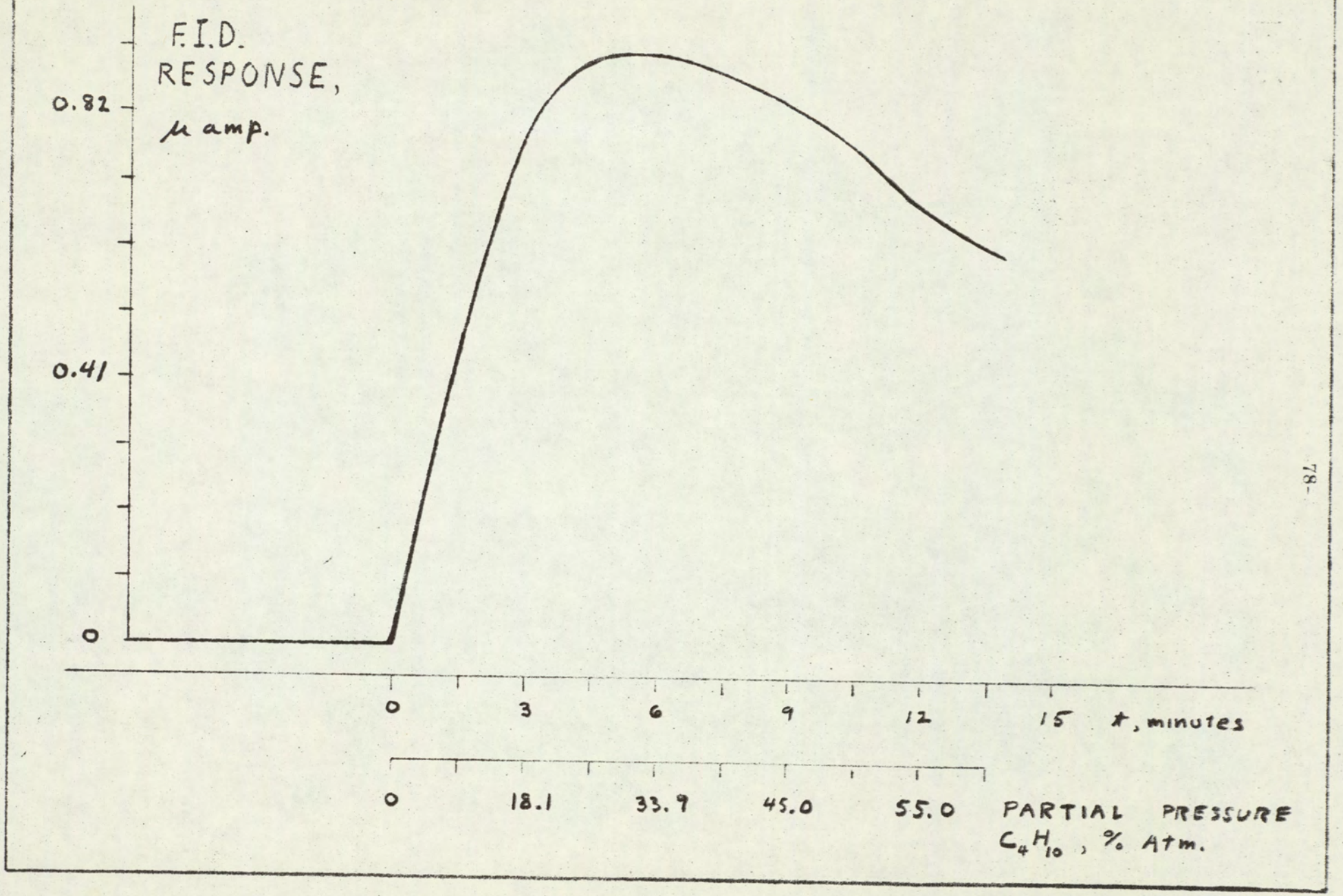

Figure 22. F. I. D. response to exponential increase in partial pressure of unburnt butane.

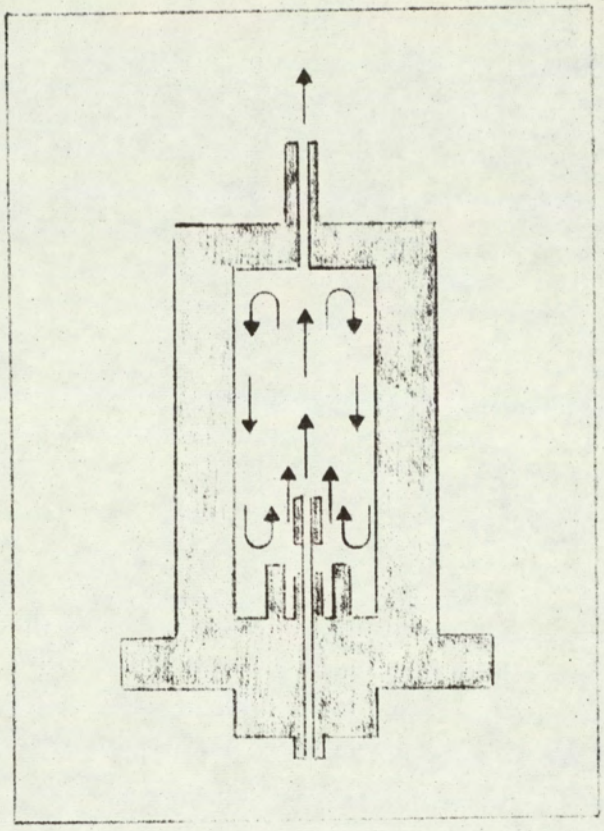

Figure 23. Mixing chamber effect in F.I.D.
Exhaust products are mixed into air supply.

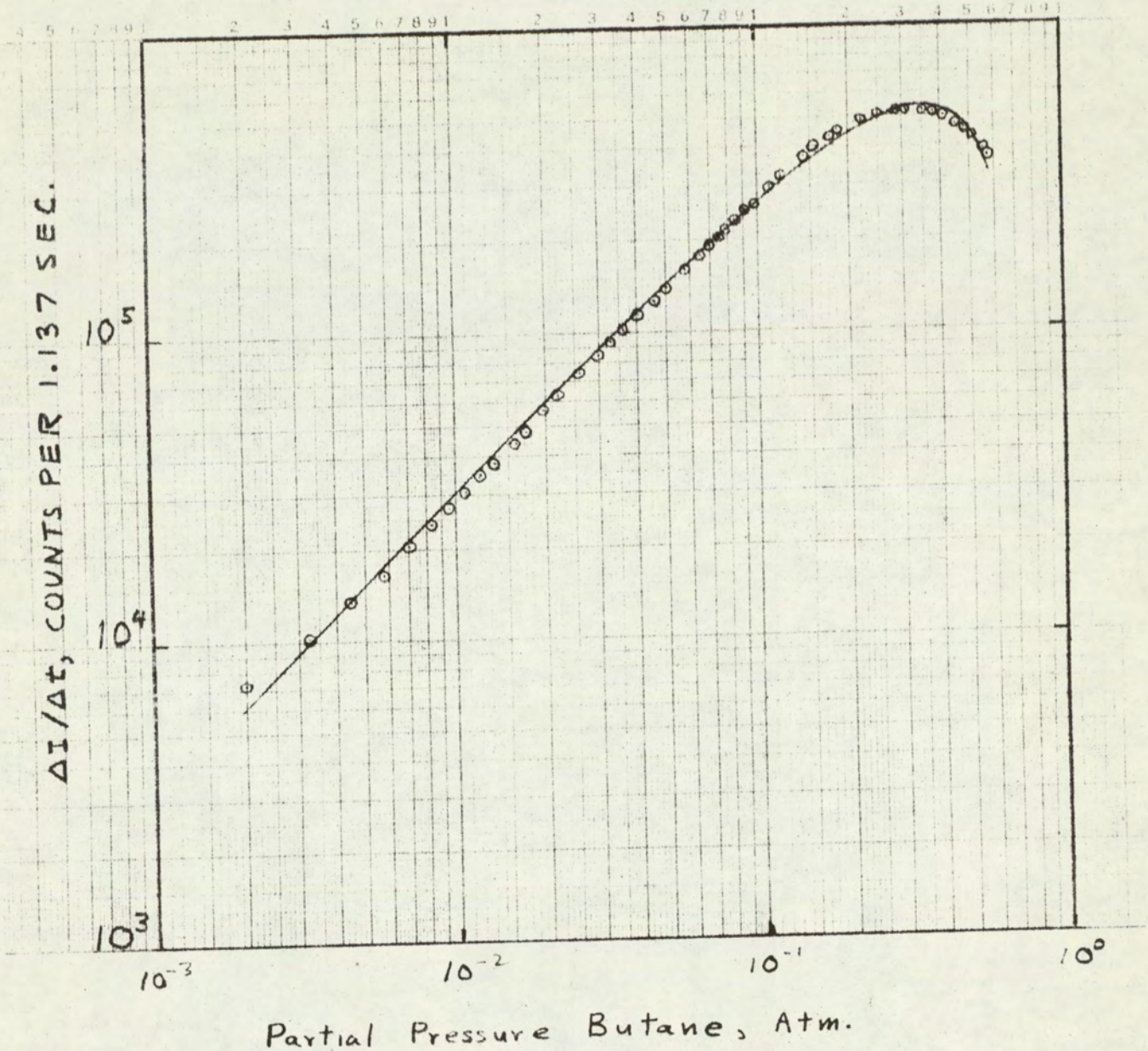

Figure 24. Least squares fit response curve and butane response data.

APPENDIX I

Reference (34)

Equation (22) can be written

$$p = (r_o/R_o)^2 P - p_o/i + \frac{2 r_o P E(r,z)}{R_o^2},$$

where

$$E(r,z) = \sum \frac{J_1(uR_o) J_o(ur)}{u[J_o(uR_o)]^2} \exp\left(-ku^2 z/i\right), \tag{I-1}$$

and where the summation is over all values of u that satisfy $J_1(uR_o) = 0$. The n^{th} root of $J_1(x)$ is given approximately by

$$x_m = \pi\left\{m + \frac{1}{4} - \frac{0.151982}{4m+1} + \frac{0.015399}{(4m+1)^3} - \frac{0.245270}{(4m+1)^5}\right\} \tag{I-2}$$

the summation in (I-1), therefore, is over all values of $u = x_n/R_o$, $n = 1, 2, 3 \ldots$

In general, Bessel functions of the first kind can be described by

$$J_\ell(x) = \frac{(x/2)^\ell}{\ell!}\left\{1 + \sum_{k=1}^{\infty} \frac{(-1)^k (x/2)^{2k} \ell!}{k!\,(\ell+k)!}\right\} \tag{I-3}$$

from which we get

$$J_o(x) = 1 + \sum \frac{(-1)^k (x/2)^{2k}}{(k!)^2} \tag{I-4}$$

$$J_1(x) = (x/2)\left\{1 + \sum \frac{(-1)^k (x/2)^{2k}}{k!\,(1+k)!}\right\} \tag{I-5}$$

It appears, therefore, that the evaluation of (I-1) requires the evaluation of three infinite series. We will now attempt to determine the number of terms necessary for a "reasonable" estimate of the values of these series.

For x = any real number, ξ, there exists a positive integer, η, such that $k > \eta$ implies that the terms in the summation of (I-4) are less than unity. That is,

$$(\xi/2)^{2k}/(k!)^2 < 1, \quad \text{for } k > \eta \tag{I-6}$$

APPENDIX I

For sufficiently large k, say $k \geq 10$, we can use Stirling's approximation for k!

$$k! \approx e^{-k} k^{k} \sqrt{2\pi k} \tag{I-7}$$

(I-7) and (I-6) combine to give

$$\frac{(3e/2)^{2k/(2k+1)}}{(2\pi)^{1/(2k+1)}} < k \tag{I-8}$$

However, for large k, we can write

$$(2\pi)^{1/(2k+1)} \approx 1, \qquad 2k/(2k+1) \approx 1$$

with these approximations (I-8) becomes

$$3e/2 < k \tag{I-9}$$

Therefore, the terms in (I-4) are less than unity when k is greater than $\eta = \chi e/2$.

Consider the ratio, $\mathcal{R}$, of the absolute value of the $(k+1)^{th}$ term to the absolute value of the k^{th} term in (I-4), when k satisfies (I-9).

$$\mathcal{R} = \frac{(\chi/2)^{2k+2}(k!)^2}{(\chi/2)^{2k}[(1+k)!]^2} = \left(\frac{\chi/2}{k+1}\right)^2$$

$$\mathcal{R} \leq \left(\frac{\chi/2}{\chi e/2 + 1}\right)^2 = \left(\frac{1}{e + 2/\chi}\right)^2 \leq 0.135, \quad \text{for } \chi > 0 \tag{I-10}$$

According to (I-10), if k is large enough for the absolute value of the k^{th} term in (I-4) to be less than unity, then the absolute value of the $(k+1)^{th}$ term is less than or equal to 13.5% of the k^{th} term. If we can assume that k is large enough for the k^{th} term to represent a 10% correction or less to the <u>total</u> summation, then the $(k+1)^{th}$ term represents approximately a 1% correction or smaller to the total summation. The above analysis can be used to show that the $(k+2)^{th}$

APPENDIX I

term represents a 13.5% correction or less to the $(k + 1)^{th}$ term, and so on. Therefore, the series, whose summation appears in (I-4) converges rapidly for terms smaller in absolute value than unity.

For the purposes at hand, J_o (x) will be evaluated by summing over $1 \leq k \leq$ INT ($x\mathbf{e}/2 + 5$), where the upper limit is the nearest integer to $x\mathbf{e}/2 + 5$. The same values of k will suffice for the evaluation of J_1 (x) also, since k! (1 x k)! in the denominator of (I-5) implies that J_1 (x) converges faster than J_o (x). That is, $k!\ (1 + k)! > \left[k!\right]^2$.

The program on page 84 computes E (r, z). At the flame front the partial pressure of fuel, p, is equal to zero. Using the computed values of E (r, z) and equation (22), we get

$$i P_f / P_o = R_o^2 / [r_o (2E + r_o)] - 1 \quad , \qquad \text{(I-11)}$$

where we have used the definition of $\mathbf{p}$ given in the text. Figure 10 is a plot of (I-11) for the case $R_o = 0.2$ cm., $r_o = 0.019$ cm.

COMPUTER PROGRAM

written in "basic"

Notation:

R = R_o

L = r_o

D = k

V = $\dot{z}$

U = n^{th} root of J_1 (x)

A (N) = J_o (uR_o)

B (N) = J_1 (ur_o)

C (N, J) = J_o (ur)

E (J, p) = E (r, z)

x = r

y = z

APPENDIX I

```
005 DIM A(12),B(12),C(12,10)
010 READ R,L,D,V,X1,Y1
020 FOR N=1 TO 10
030 LET U1=N+.25-.151982/(4*N+1)+.015399/(4*N+1)↑3
040 LET U2=.24527/(4*N+1)↑5
050 LET U=(U1-U2)*3.1416
060 LET S1=0
070 LET S2=0
080 LET F=1
090 LET F1=1
093 LET Z1=1
095 LET Z2=1
100 FOR K=1 TO INT(U*1.4+5)
110 LET F=F*K
120 LET F1=F1*(K+1)
123 LET V1=ABS(Z1)
125 IF V1<(10)↑(-20) THEN 138
130 LET Z1=(-1)↑K*((U/2)↑K/F)↑2
135 LET S1=S1+Z1
136 LET V2=ABS(Z2)
138 IF V2<(10)↑(-20) THEN 170
140 LET Z2=(-1)↑K/(F*F1)*(.5*U*L/R)↑(2*K)
160 LET S2=S2+Z2
170 FOR I=1 TO X1
180 LET X(I)=0
190 IF K=1 THEN 210
200 GO TO 215
210 LET T(I)=0
212 LET H(I)=1
215 LET L(I)=ABS(H(I))
218 IF L(I)<(10)↑(-20) THEN 235
220 LET H(I)=(-1)↑K*((.5*U*X(I)/R)↑K/F)↑2
230 LET T(I)=T(I)+H(I)
```

Continued on Page 85

APPENDIX I

```
235 NEXT I
240 NEXT K
250 LET A(N)=1+S1
260 LET B(N)=.5*(1+S2)*U*L/R
265 LET Z=0
270 FOR J=1 TO X1
280 LET C(N,J)=1+T(J)
290 FOR P=1 TO Y1
300 LET Y(P)=.1*P
310 IF N>1 THEN 350
320 LET E(J,P)=B(1)*C(1,J)*R/(U*A(1)↑2)*EXP(-D*(U/R)↑2*Y(P)/V)
330 GO TO 450
350 LET G=B(N)*C(N,J)*R/(U*A(N)↑2)*EXP(-D*(U/R)↑2*Y(P)/V)
352 LET E(J,P)=E(J,P)+G
354 LET W(J,P)=ABS(G/E(J,P))
355 IF W(J,P)<.001 THEN 370
360 GO TO 450
370 LET Z=Z+1
380 IF Z=X1*Y1 THEN 478
450 NEXT P
460 NEXT J
470 NEXT N
478 PRINT "N=";N
480 FOR Q=1 TO X1
490 FOR S=1 TO Y1
500 PRINT "X=";X(Q);"Y=";Y(S);"E=";E(Q,S)
505 PRINT "ABS(DELTA(E)/E)=";W(Q,S)
510 NEXT S
520 PRINT
530 NEXT Q
600 DATA .2,.019,.65,730,1,10
700 STOP
```

APPENDIX I

To use program:

Line No. 600 is a data input statement. From left to right the numbers refer to the air conduit radius, jet radius, coefficient of interdiffusion, linear gas velocity, the number of radial coordinates, and the number of vertical coordinates for which E (r, z) is to be computed. For each value of N, the n^{th} root of $J_1(x)$ is computed (statements 030, 040, 050). The Bessel functions J_o (ur), J_o (uR_o), and J_1 (ur_o) are computed by using the finite number of terms determined by statement 100. Each value of N corresponds to a term in the expression for E in (I-1). As many as ten terms will be used to compute E. However, if the N_1^{th} term represents a 0.1% correction or less to the summation of the first N_1-1 terms, and if it does so for all the radial and vertical coordinates simultaneously, then the evaluation of E is terminated (statements 265, 355, 370, 380).

Print-Out:

The two columns on the left of Page 87 are the results of the program on Page 84. N=8 indicates that the evaluation of E did not require the full ten terms allotted for (I-1). x = o means that we have computed E along the flame axis (i.e., r = o). ABS (Delta (E) / E) is the absolute value of the correction to E that was made by the final (N=8) term.

APPENDIX I

```
N= 8
X= 0 Y= .1    E= .544007
ABS(DELTA(E)/E)= 5.95785E-05
X= 0 Y= .2    E= .380652
ABS(DELTA(E)/E)= 1.91193E-05
X= 0 Y= .3    E= .284551
ABS(DELTA(E)/E)= 5.74312E-06
X= 0 Y= .4    E= .223806
ABS(DELTA(E)/E)= 1.63962E-06
X= 0 Y= .5    E= .182908
ABS(DELTA(E)/E)= 4.50494E-07
X= 0 Y= .6    E= .153862
ABS(DELTA(E)/E)= 1.20253E-07
X= 0 Y= .7    E= .132308
ABS(DELTA(E)/E)= 3.14013E-08
X= 0 Y= .8    E= .11573
ABS(DELTA(E)/E)= 8.06112E-09
X= 0 Y= .9    E= .102602
ABS(DELTA(E)/E)= 2.04168E-09
X= 0 Y= 1.    E= 9.19582E-02
ABS(DELTA(E)/E)= 5.11520E-10
```

$i P_f/P_o$	$k\bar{z}/\dot{z}$
0.90	0.89×10^{-4} cm^2
1.69	1.78
2.59	2.67
3.51	3.56
4.47	4.45
5.44	5.34
6.44	6.23
7.39	7.12
8.35	8.01
9.37	8.90 ↓

For the case of ion diffusion we have a single species (no distinction was made between positive and negative ions) diffusing radially in a gas that is inert as far as charge neutralization is concerned (recombination was treated as an independent mechanism). Therefore, we can replace p_f and p with n_o and n, the ion densities in and above the flame respectively. Since there is no "chemical" reaction with the gas into which the ions are diffusing, the appropriate value for p_o is zero. Equation (22) can now be written as

$$m = (n_o/R_o)^2 m_o + 2 n_o m_o E / R_o^2 \qquad \text{(I-12)}$$

$$m/m_o = (n_o/R_o)^2 \left\{ 1 + 2E/n_o \right\} \qquad \text{(I-13)}$$

where (I-13) is an expression for the relative ion density as a function of the computer evaluated quantity, E. On Page 88 we see the modifications that

APPENDIX I

were made to the program on Page 84 in order to perform the ion diffusion analysis. The results of this analysis are shown below.

```
600 DATA .3,.0455,.035,434,10,4
180 LET X(I)=(I-1)*R/10
300 LET Y(P)=9.52+(P-1)*12.7
RUN


N= 8
X= 0 Y= 9.52 F= .461206
ABS(DELTA(E)/E)= 1.16668E-07
X= 0 Y= 22.22  F= .225342
ABS(DELTA(E)/E)= 1.15278E-10
X= 0 Y= 34.92  F= .143291
ABS(DELTA(E)/E)= 8.75206E-14
X= 0 Y= 47.62  F= .101949
ABS(DELTA(E)/E)= 5.93862E-17

X= .03  Y= 9.52 F= .371591
ABS(DELTA(E)/E)= 1.33596E-08
X= .03  Y= 22.22  F= .199874
ABS(DELTA(E)/E)= 1.19907E-11
X= .03  Y= 34.92  F= .131635
ABS(DELTA(E)/E)= 8.78963E-15
X= .03  Y= 47.62  F= 9.53077E-02
ABS(DELTA(E)/E)= 5.86075E-18

X= .06  Y= 9.52 F= .187566
ABS(DELTA(E)/E)= 3.35329E-08
X= .06  Y= 22.22  F= .138012
ABS(DELTA(E)/E)= 2.20013E-11
X= .06  Y= 34.92  F= .101338
ABS(DELTA(E)/E)= 1.44655E-14
X= .06  Y= 47.62  F= 7.74284E-02
ABS(DELTA(E)/E)= 9.14001E-18

X= .09  Y= 9.52 F= 4.79531E-02
ABS(DELTA(E)/E)= 2.48145E-07
X= .09  Y= 22.22  F= 7.05196E-02
ABS(DELTA(E)/E)= 8.14615E-11
X= .09  Y= 34.92  F= 6.34424E-02
ABS(DELTA(E)/E)= 4.37142E-14
X= .09  Y= 47.62  F= 5.34344E-02
ABS(DELTA(E)/E)= 2.50566E-17

X= .12  Y= 9.52 F=-8.04503E-03
ABS(DELTA(E)/E)= 1.64086E-06
X= .12  Y= 22.22  F= 2.06263E-02
ABS(DELTA(E)/E)= 3.08971E-10
X= .12  Y= 34.92  F= 2.89662E-02
ABS(DELTA(E)/E)= 1.06215E-13
X= .12  Y= 47.62  F= 2.91673E-02
```

APPENDIX I

```
X= .15  Y= 9.52 F=-2.07267E-02
ABS(DELTA(F)/F)= 5.27832E-07
X= .15  Y= 22.22   F=-6.62211E-03
ABS(DELTA(F)/F)= 7.97571E-10
X= .15  Y= 34.92   F= 4.03869E-03
ABS(DELTA(F)/F)= 6.31343E-13
X= .15  Y= 47.62   F= 8.94864E-03
ABS(DELTA(F)/F)= 1.37559E-16

X= .18  Y= 9.52 F=-2.27437E-02
ABS(DELTA(F)/F)= 2.74478E-07
X= .18  Y= 22.22   F=-.017971
ABS(DELTA(F)/F)= 1.67702E-10
X= .18  Y= 34.92   F=-1.07784E-02
ABS(DELTA(F)/F)= 1.34987E-13
X= .18  Y= 47.62   F=-5.41103E-03
ABS(DELTA(F)/F)= 1.29810E-16

X= .21  Y= 9.52 F=-2.27129E-02
ABS(DELTA(F)/F)= 4.11452E-08
X= .21  Y= 22.22   F=-.021625
ABS(DELTA(F)/F)= 2.08629E-11
X= .21  Y= 34.92   F=-1.81371E-02
ABS(DELTA(F)/F)= 1.20089E-14
X= .21  Y= 47.62   F=-1.42441E-02
ABS(DELTA(F)/F)= 7.38203E-18

X= .24  Y= 9.52 F=-2.27195E-02
ABS(DELTA(F)/F)= 1.73266E-07
X= .24  Y= 22.22   F=-2.25393E-02
ABS(DELTA(F)/F)= 8.43162E-11
X= .24  Y= 34.92   F=-2.12141E-02
ABS(DELTA(F)/F)= 4.32481E-14
X= .24  Y= 47.62   F=-1.89687E-02
ABS(DELTA(F)/F)= 2.33504E-17

X= .27  Y= 9.52 F=-2.27934E-02
ABS(DELTA(F)/F)= 1.16605E-07
X= .27  Y= 22.22   F=-2.27177E-02
ABS(DELTA(F)/F)= 5.64808E-11
X= .27  Y= 34.92   F=-2.22864E-02
ABS(DELTA(F)/F)= 2.77950E-14
X= .27  Y= 47.62   F=-2.10974E-02
ABS(DELTA(F)/F)= 1.41748E-17
```

APPENDIX I

The data necessary for plotting figures 16 and 17 can now be computed. Below are the results for z = 47.62 cm.

x	E	n/n_o	r/R_o	$(r/R_o)^2$
0	1.019×10^{-1}	1.26×10^{-1}	0	0
0.03	9.531×10^{-2}	1.19×10^{-1}	0.1	0.01
0.06	7.743×10^{-2}	1.01×10^{-1}	0.2	0.04
0.09	5.343×10^{-2}	7.70×10^{-2}	0.3	0.09
0.12	2.917×10^{-2}	5.25×10^{-2}	0.4	0.16
0.15	8.949×10^{-3}	3.21×10^{-2}	0.5	0.25
0.18	-5.411×10^{-3}	1.76×10^{-2}	0.6	0.36
0.21	-1.424×10^{-2}	8.66×10^{-3}	0.7	0.49
0.24	-1.897×10^{-2}	3.90×10^{-3}	0.8	0.64
0.27	-2.110×10^{-2}	1.70×10^{-3}	0.9	0.81
0.30		0	1.0	1.0

APPENDIX II

$n_o(t)$ is the ion density in the flame in cm^{-3} and is a function of time, t.

$\frac{n}{n_o}(z,r)$ is the relative ion density z cm above the flame and is a function of the radial coordinate, r, but is not a function of t.

$2\pi\, r\, dr\, dz$ is a differential volume element in cylindrical coordinates.

Therefore

$$n_o(t)\,\frac{n}{n_o}(z,r)\,2\pi r\,dr\,dz$$

is the total number of ions in volume which lies between z and z + dz and between r and r + dr.

The total number of particles between z and z + dz is given by

$$n_o(t)\,2\pi\,dz\int_0^{R_o}\frac{n}{n_o}(z,r)\,r\,dr = n_o(t)\,\pi r_o^2\,dz\,, \quad \text{for } z = 0$$

The fraction of flame ions which reach height z is given by:

$$\frac{n_o(t)\,2\pi\,dz\int_0^{R_o}\frac{n}{n_o}(z,r)\,r\,dr}{n_o(t)\,\pi r_o^2\,dz}$$

$$= 1, \text{ for } z \leq 47.62 \text{ cm} \quad \text{(See text)}$$

The number in z to z + dz and $0 \leq r \leq r_1$ is

$$N = n_o(t)\,2\pi\,dz\int_0^{r_1}\frac{n}{n_o}(z,r)\,r\,dr$$

The fraction in z to z + dz and $0 \leq r \leq r_1$ is

$$F = \frac{2}{r_o^2}\int_0^{r_1}\frac{n}{n_o}(z,r)\,r\,dr \qquad \text{(II 1)}$$

$$N = n_o(t)\,2\pi\,r_1\,dz\,F$$

Let $\frac{n}{n_o}(z,r) = A\exp\left[-B\,(r/R_o)^2\right]$ (II 2)

where A and B are functions of z

APPENDIX II

$$F = (2/r_o^2)\int_0^{r_1} A \exp\left[-B\,(r/R_o)^2\right] r\, dr \qquad \text{(II 3)}$$

$$= \frac{A}{B}\left(\frac{R_o}{r_o}\right)^2 \left\{ 1 - \exp\left[-B\,(r_1/R_o)^2\right] \right\} \qquad \text{(II 4)}$$

For $F = 1$ and $B\,(r_1/R_o)^2 >> 1$

We get $A/B = (r_o/R_o)^2$ (II 5)

Combining(II-4) and (II-5) we get equation (73)

AVERAGE VELOCITY IN LAMINAR FLOW

Linear velocity as function of radius is given by

$$\dot{z}(r) = 2\dot{z}_o\,(1-(r/R_o)^2) \qquad \text{Equation (68)}$$

Let $\overline{\dot{z}(r_1)}$ = average velocity of particles in $0 \le r \le r_1$ AND z to $z + dz$

$$\overline{\dot{z}(r_1)} = \frac{\int_0^{r_1} m_o(t)\,\frac{m}{m_o}(z,r)\,2\pi r\left[2\dot{z}_o\left(1-(r/R_o)^2\right)\right] dz\, dr}{\pi r_o^2\, m_o(t)\, dz} \qquad \text{(II 6)}$$

For Gaussian distribution in (II 2) we get

$$\overline{\dot{z}(r_1)} = \frac{4A\dot{z}_o}{r_o^2}\int_0^{r_1} r\,(1-(r/R_o)^2)\exp\left[-B\,(r/R_o)^2\right] dr \qquad \text{(II 7)}$$

$$= 2\dot{z}_o\left\{(2/r_o^2)\int_0^{r_1} A\exp\left[-B\,(r/R_o)^2\right] r\, dr + \right.$$

$$\left. -(2A/r_o^2)\int_0^{r_1}\frac{r^3}{R_o^2}\exp\left[-B\,(r/R_o)^2\right] dr \right\} \qquad \text{(II 8)}$$

$$\overline{\dot{z}(r_1)} = 2\dot{z}_o\left\{ F - \left(\frac{R_o}{r_o}\right)^2\frac{A}{B^2}\left[B\,(r_1/R_o)^2+1\right]\exp\left[-B\,(r_1/R_o)^2\right] - 1 \right\} \qquad \text{(II 9)}$$

Where F is given in (II 4)

APPENDIX II

When (II-5) is valid we can write:

$$\overline{\dot{\varepsilon}}(r_1) = 2\dot{\varepsilon}_0 \left\{ 1 + \frac{\left[(r_1/R_0)^2 + 1/B \right] \exp\left[-B (r_1/R_0)^2 \right] - 1/B}{1 - \exp\left[-B (r_1/R_0)^2 \right]} \right\}$$

Equation (74)